ACIPET

Enhanced Carbon Storage Process from Flue Gas Streams Using Rice-Husk Silica Nanoparticles: An Approach in Shallow Coal Bed Methane Reservoirs.

Autor(es): O. E. Medina, L. J. Giraldo, F. B. Cortés, and C. A. Franco. Universidad Nacional de Colombia – Sede Medellín.

Categoría: Marque con una "X"

• Artículo Técnico	X
• Tesis Pregrado	
• Tesis Posgrado	

Abstract

Carbon capture and storage (CCS) is considered a key process to reach net-zero emission by 2050 aim limiting global warming. Coal Beds Methane (CBM) are considered potential geological reservoirs for underground CCS due to the CO_2-CH_4 exchange feasibility by adsorptive phenomena. It is worth mentioning that global implementation has been focused only on deep reservoirs to provide methane recovery. Thus, this work proposes a modified CCS process based on silica nanoparticle inclusion for shallow CBM reservoirs (<300 m). The nanomaterials were evaluated at high pressure in two main stages including *i*) CO_2 sorption on a single CO_2 stream and *ii*) CO_2 selectivity on a flue gas stream (N_2-CO_2 mixture). This work includes silica nanomaterial synthesized from rice husk as agro-waste sources with better technical-economic feasibility framed in a circular economy to reduce costs and maximize the use of available resources. Rice husk silica nanoparticles (RSi) were doped with 1.0, 3.0, and 5.0 wt.% of urea (Si-U), diethylamine (Si-DE), triethylamine (Si-TE), and ethylenediamine (Si-EM) to enhance the CO_2 sorption. First, CO_2 sorption was evaluated at 30 °C and between 0.084 MPa and 3 MPa using a CO_2 stream to determine the best-doped amount of each N-source. Then, the best nanoparticles were used to impregnate CBM at 10 wt.% and 20 wt.%, and the subsequent CO_2 storage on the flue gas stream (70 %v/v N_2 and 30 %v/v CO_2) was done. The results showed that CO_2 sorption on RSi increases with the N-group coating in the order RSi-DE < RSi-TE < RSi-U < RSi-EM. Also, the best-doped amount for each N-source was 3 wt.%. For CBM impregnation, the nanofluid containing 20 wt.% of RSi-EM3 presented the best yield increasing the CO_2 sorption from 0.05 to 0.75 mmol g^{-1}, meaning an increase of more than 1000% in the sorption capacity.

Introduction

Carbon dioxide (CO_2) is considered the primary contributor to greenhouse gases (GHG) compared to other gases like methane, nitrous oxides, and ozone, among others.[1] The concentration of CO_2 in the atmosphere has been observed to constantly rising mainly associated with the burning of fossil fuels to satisfy the global demand for energy, which accounts for around 81% of the world's commercial energy supply.[2] The excess emission of CO_2 to the atmosphere is the main reason for the current global climate change and its associated problems, including global warming, sea-level rise, and ocean acidification, threatening human development.[3] Thus, alternatives to reducing and controlling CO_2 emissions towards mitigating climate change must be developed and deployed. In this context, alternatives like Carbon, Capture, and Storage (CCS) are acknowledged as an important strategy toward a net-zero-CO_2 emission pathway,[4] which offers the possibility of using existing technologies to achieve a net-negative-CO_2 emission.[5, 6] CCS processes are considered a feasible approach to reducing CO_2 emissions.[7] It is featured as the second-largest contributor to the mitigation of GHG emissions by 2050 according to the Organization for Economic Co-operation and Development and the International Energy Agency.[8]

About the CCS strategies are widely recognized the Coal Bed Methane (CBM) reservoirs, which includes methane recovery processes based in a gas exchange of CO_2-Methane due to its great affinity for carbon adsorption onto the coal bed.[9] CCS processes related to CBM reservoirs are coupled to Methane production that promotes a subsequent carbon storage then of methane recovery, being this process commonly developed in deep depth with particular characteristics of CO_2 state and some specific facilities for their injection

to the underground.[9] The amount of CO_2 that can be stored in subsurface mostly depends of reservoir conditions like pressure, temperature, and particular petrophysics of the coal.[9, 10] According to specialized literature, a suitable reservoir for CO_2 storage should be located in deep depth (approximately between 300 to 1500 m) to assure acceptable adsorption of the gas on the coal.[11, 12] However, in several countries also are reported wide areas with depleted or unmineable coal beds located at shallow depth that under certain conditions could be a good alternative to promote the carbon sequestration. Particularly, in Colombia are described several carboniferous formations of coal bed at shallow deep around < 300 m, which eventually could have good prospect to be used in CCS process.[13, 14]

Considering that the sorption phenomena is the driver mechanism of CCS on CBM reservoirs,[15-17] nanotechnology can be considered as a great option to enhance this process with the inclusion of nanomaterials which have exclusive properties including low sorbent cost, high selectivity, simplicity of design, regeneration, and high surface energy.[18-23] Big efforts have been done by several authors on the synthesis and application of nanomaterials for CO_2 storage focused on sandstone-based reservoirs. Rodriguez et al.[24, 25] were the pioneers on this technology by the development of carbonaceous nanomaterials for CO_2 capture from flue gas streams applied to shallow sandstone reservoirs. The authors obtained that sandstone adsorptive capacity increased from 0.0013 mmol g^{-1} (non-treated) up to 0.64 mmol g^{-1} (impregnated with 20 wt.% of carbon nanoparticles). Similarly, many nanomaterials have been developed to enhance the efficiency of CO_2 sorption commonly used in surface facilities, including zeolites,[26-28] metal-organic frameworks (MOFs),[29-32] carbon-based and alumina-silicate nanomaterials,[33-37] among others.[24, 25, 38] Pham et al.[18] developed nano-zeolites with a CO_2 adsorption capacity of 4.81 mmol g^{-1} (at 20 °C and 1 atm). Regarding Metal-organic frameworks materials, a wide variety is reported in the literature with several differences in their structure and composition corresponding to a wide range of CO_2 capture efficiency with reported average values of CO_2 adsorption from 0.3 up to 6.0 mmol g^{-1} or even higher depending on the composition and conditions of pressure and temperature, such as is described by Ding et al.[31] and Ghanbari et al.[32] Between them, silica-based nanomaterials have many advantages associated to their chemical stability, simple synthesis and high surface area.[39, 40] In recent years, researchers such as Li et al.[41] studied the influence of silica types in the performance and synthesis by grafting amine-silica hybrid materials used for post-combustion CO_2 capture. Moreover, Wu et al.[42] synthesized four silica-based nanomaterials, including magnesium silicate ($MgSiO_3$), manganese silicate ($MnSiO_3$), copper silicate ($CuSiO_3$), and zirconium silicate ($ZiSiO_3$), from coal gangue via hydrothermal method performing a strong selectivity towards CO_2 over N_2, which can be used like start point in the storage process of CO_2 in CBM.

On the other hand, some researches has established silica-modified nanomaterials such as amine-functionalized as ideal sorbents for selective separation of CO_2 from a mixture of gases due to their reversible reaction with CO_2.[43] The interaction between acidic CO_2 and other molecules as basic amine groups could increase the CO_2 uptake, enhancing their sorption capacity, which have been widely studied in the scientific literature in capture process.[44-47] Although the silica nanomaterials developed in the literature mentioned above were not applied for carbon storage in reservoir of sandstone and CBM. These have tunable characteristics have the great potential to be involved in this kind of process. Additionally, to promote an environmentally friendly process with a minor footprint carbon. To the best of our knowledge, this is the first study using amine-functionalized biomass-derived silica nanoparticles to improve the chemical-physical properties of Carbon Beds Methane to enhance their CO_2 selective sorption based on a CCS process.

Therefore, the aim of this work also included the development of biomass-derived silica nanomaterials from rice-husk for being used to enhance the CO_2 storage from flue gas streams in shallow reservoirs of CBM. In this sense, this work aimed to assess the potential of carbon sequestration in shallow CBM reservoirs based in the biomass-derived silica nanoparticles inclusion by enhanced sorptive phenomena. To this aim, silica nanoparticles were synthesized using rice husk and subsequent doped with four nitrogen-sources (3 amines and urea) at 1 wt.%, 3 wt.% and 5 wt.%. The nanoparticles were robustly characterized and evaluated in CO_2 sorption to then, select the best dosage of each source and impregnate the CBM at 10 and 20wt.%. Finally, CO_2 storage capacity on CBM was measured using flue gas streams (N_2-CO_2 mixture).

Experimental

Materials.

Biomass-derived silica nanoparticles were used for this study. Rice husk from a local Colombian mill was used to synthesize the silica nanoparticles. Additionally, regents as chloride acid (37% purity) and sodium hydroxide (98% purity) were purchased from Merck KGaA (Darmstadt, Germany), sulfuric acid (98% purity) was obtained from PanReac AppliChem (Darmstadt, Germany), all used to synthesize silica nanoparticles. Furthermore, for surface modification the following chemicals were used, all from Sigma-Aldrich (St. Louis, MO): urea (99% purity), diethylamine (99% purity), triethylamine (99% purity), and ethylenediamine (99% purity). Figure 1 shows the chemical structure of the surface modifiers.

a) $(CO(NH_2)_2)$ b) $(C_2H_4(NH_2)_2)$

c) $((CH_3CH_2)_2NH)$ d) $(N(CH_2CH_3)_3)$

Figure 1. Chemical structure of the surface modifiers a) urea, b) ethylenediamine, c) diethylamine, and d) triethylamine.

Carbon bed methane (CBM) sample was taken from a Colombian outcrop located in Guajira basin and was impregnated with nanoparticles for the CO_2 sorption tests. The CBM sample presents a total organic content (TOC) of 16.6 wt.%. The ash content (associated to the inorganic carbon) was stabilized in 67.4 wt.%. The surface area of CBM sample was 13.672 $m^2\ g^{-1}$. The remainder of the sample is considered non-purgeable organic carbon. Also, the humidity was 8.10%.

Methods

Figure 2 shows the proposed workflow to develop and evaluate CO_2 sorption and selectivity over nanoparticles doped on carbon bed methane samples. The process starts with the rice-husk silica (RSi) synthesis and impregnation with four nitrogen sources at 1 wt.%, 3 wt.% and 5 wt.%. The systems are evaluated on CO_2 sorption between 0.084 MPa and 3.0 MPa to select the best-in-class nanoparticles and make de subsequent impregnation of CBM. The CBM was doped with 10 wt.% and 20 wt.% of nanoparticles and its CO_2 sorption on the flue gas stream was assessed.

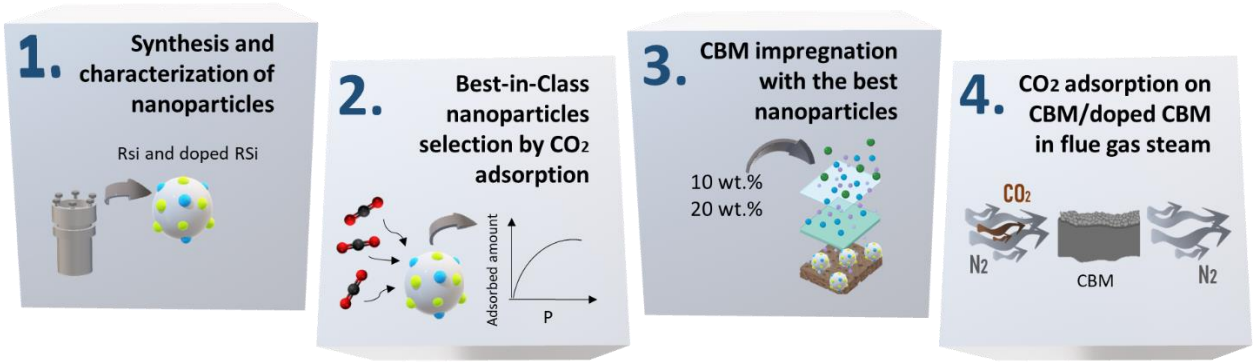

Figure 2. Conducted workflow in this research.

Synthesis of silica nanoparticles. The rice-husk silica (RSi) synthesis was developed based on the methodology proposed by Ghorbani et al.[48], with some variations reported by Montes et al.[49]. The synthesis starts with collecting the rice husks and subsequent washing with deionized water to remove dirt and impurities and further drying at 90˚C for 1 h to remove humidity. Then, a pretreatment with HCl 1M for 2 h at 80 °C was carried out. The rice husk was further rewashed to remove heavy elements, and it was calcined at 600 °C for 6 h. The obtained ashes were treated with a basic solution of NaOH 0.5N at 90 °C under vigorous stirring for 6 h. The solution was filtered and neutralized with H_2SO_4 15% to reach a pH of 8. The obtained gel was left to stand for 24 h and further centrifuged at 4500 rpm. The material was filtered and washed with deionized water to remove the excess and impurities, then finally dehydrated, and calcined at 600°C to obtain the silica nanoparticles.

Surface modification of nanoparticles. The modifications were performed with four nitrogen compounds agents, such as Urea, Ethylenediamine, Triethylamine, and Diethylamine, through the incipient impregnation methodology.[50] For this, different stock solutions with each agent at a mass fraction of 1, 3, and 5 wt.% regarding the mass of nanomaterial were prepared. After impregnation, the modified nanoparticles were washed with deionized water in excess, obtaining a total determined amount impregned onto the nanomaterial surface by a posterior thermogravimetric analysis.

Characterization of nanoparticles. Silica and modified silica nanoparticles were characterized by different techniques to determine the textural and chemical properties. The material's surface was estimated from nitrogen adsorption/desorption isotherms at -196.15 °C on a Quantachrome Autosorb-1 equipment after outgassing samples overnight.[51] The surface area of was calculated using the Brunauer-Emmett-Teller (BET) method.[52] The BET model describes multimolecular adsorption for a solid-gaseous system, applying the Langmuir equation for the different adsorbate layers on the sorbent.[53, 54 55, 56] The hydrodynamic diameter was determined by through the dynamic light scattering (DLS) using a NanoPlus-3 (Micromeritics, GA, USA)dispersing the nanoparticles in an aqueous solution. The mean particle size was calculated from the diffusional properties of the particle, indicating the size of the hydrated and solvated particle. Stokes' Law provides a convenient method for determining particle size distribution (PSD).[57] Scanning electron microscopy (SEM) was used to obtain the dry particle size and morphology of the samples. The analysis was carried out using a GEMINI-LEO1530 VP FE-SEM emission electron microscope (Carl Zeiss, Cambridge, UK).

The decomposition of the different synthesized materials was evaluated as a function of temperature to determine the experimental impregnation of the N-doped phase. Thermogravimetric analysis (TGA) was performed in Q50 equipment (TA Instruments, Inc., New Castle, DE, USA) in the presence of air atmosphere at flow rate of 100 mL min^{-1} and a heating rate of 20°C, from 30 up to 800 °C. The differences in the mass loss between the virgin material and the surface-modified (functionalized) material with adsorbed species determine the total amount adsorbed and the effectiveness grafted onto the surface.[58]

Temperature programmed desorption with NH_3 (TPD-NH_3) experiments were performed to measure the total acidity of the synthesized materials to correlate the surface acidity with the molecular interaction behavior with the CO_2/N_2 gas. Surface acidity TPD-NH_3 experiments were performed in the equipment Chembet 3000 (Quantachrome Instruments, USA) following a similar procedure used by Lopez et al.[59] Approximately 0.1 g of each prepared nanomaterial was dried at 200 °C for 1 hour under He flow in a U-shaped quartz tube. Adsorption was performed with a fixed amount of 10 vol% NH_3 in He at 80 mL min^{-1} introduced to be adsorbed at 100 °C for 1 h. The carrying gas was changed to pure He at 80 mL min^{-1} at 100°C for 1 h and finally heated up to 900°C at 10 °C min^{-1}, obtaining the desorption process. A calibrated Thermal conductivity detector (TCD) with a constant flow of He at 80 mL min^{-1} senses the changes in the gas flow through the instrument due to the desorption of the NH_3 in the heating ramp.[60, 61] The nanomaterials were characterized separately by Fourier transform infrared spectroscopy to determine their functional groups,[62] FTIR analyses were conducted to confirm the nanoparticles' characteristics and surface modification. The FTIR (Fourier transformed Infrared analysis was carried out in RAffinity-1 FTIR equipment (Shimadzu, Japan) in transmittance mode with a resolution of 2 cm^{-1} for a range of 4500-600 cm^{-1}. The samples are subjected to heating for 4 hours at 110°C to eliminate the water content present and are mixed with KBr (20% of material in KBr). For the spectrum measurement, KBr is taken as the blank. Also, X-ray photoelectron spectroscopy measurements were done to determine the functional groups distribution of the samples. To this aim a monochromatic Al-Kα source (1486.7 eV, 13 kV, 100 W) with step energy of 90 eV for general spectra and 20 eV for high-resolution spectra (O_{1s}, Si_{2p}, N_{1s}) was used. The step was 1 eV for general spectra and 0.1 eV for high-resolution spectra. Calibration of the adventitious C=C peak was done at 284.8 eV. All XPS spectra were analyzed using the XPSpeak4.1 software. Baseline corrections were made using a Shirley-type background correction. A Gaussian–Lorentzian sum function in different ratios fits the individual peak.

Impregnation of CBM samples. The CBM was modified to enhance the rock surface with the nanoparticles and increase the chemical-physical condition and molecular interactions. According to Rodriguez et al.,[63] the minimum nanoparticle percentages needed to improve the CO_2 sorption capacity are 10 wt.% and 20 wt.%. Considering this, in this work, the CBM was impregnated with the best in class nanoparticles at mass fractions of 10% and 20% by the immersion and soaking method.[63] The nanofluid was developed by dispersing the nanoparticles in deionized water and sonicated at 40 °C for 4 h. The CBM was introduced into the nanofluid at 60 °C for 24 h. This method mimicked the reservoir conditions. The modifying CBM was dried at 110 °C for 12 h.

CO_2 sorption experiments. Sorption tests were performed using the Thermogravimetric equipment HP-TGA 750 (TA Instruments Inc., Hüllhorst, Alemania), which permits different pressure and temperature conditions under CO_2 and/or N_2.[64] This experiment determines the interaction capacity of each system analyzed.

An HP-TGA 750 analyzer (Hullhorst, Germany) was used to evaluate the CO_2 sorption capacity of synthesized nanoparticles at a fixed temperature (25 °C) at a range of pressures between 0.084 MPa and 3.0 MPa based on a magnetic levitation technique. The magnetic system provided a monotone electromagnetic field capable of levitating a magnet set on the suspension shaft and sample maintainer. The device was calibrated based on temperature and weight. However, changing the heat conductivity of the gas by pressure and temperature makes temperature calibration at high-pressure conditions very challenging. Therefore, it is essential to do the Curi measurements in the entire pressure range of the device. To do the tests, first, a vacuum condition (0.00025 MPa and 120 °C) was used to clean the solid surfaces of the samples for 12 h. Then, pressure, temperature, and gas flow rate were adjusted to the initial conditions. A series of manometers and valves controlled the system pressure so that the high-pressure conditions were easily achieved. To correct the buoyancy effect of the gas flow, for each test, two different runs were accomplished with empty and solid-filled sample containers. Then, the obtained mass profile for each sample was reduced for the empty sample container.[65-72] Figure 3 shows the schematic diagram of the experimental system assembled for CO_2 sorption in flue gas streams.

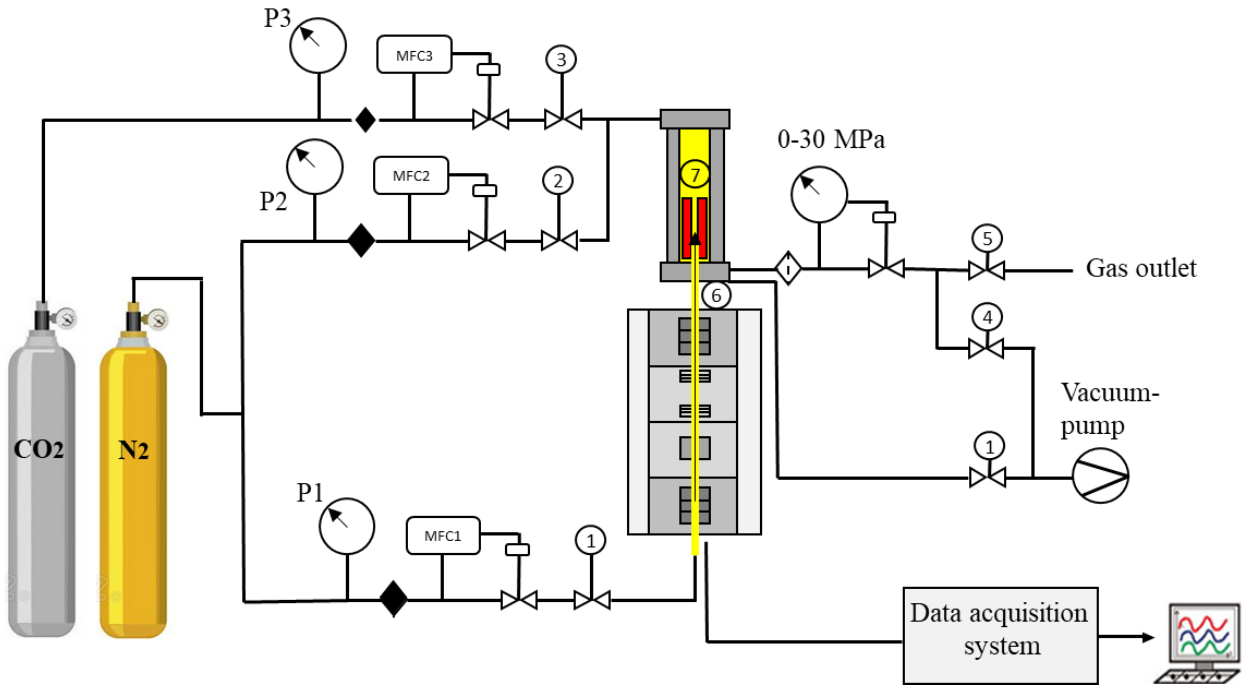

Figure 3. Schematic diagram of the experimental system assembled for CO_2 sorption in flue gas streams. MCF1-3 are the mass flow controller for each one of the gases injected into the system. P1-3 are the manometers, 1-4 are the automatic valves, 5 is the gas outlet pressure regulator, 6 is the tube balance, 7 is the magnet levitated balance and the high-pressure reaction furnace.

At high pressure, the CO_2 sorption capacity was evaluated in two different conditions: (i) under pure CO_2 (up to 3.0 MPa) using a CO_2 flow of 60 mL min^{-1} and (ii) under a CO_2/N_2 flow in (up to 3.0 MPa). The model flue gas comprising 70% N_2 and 30% CO_2 was selected. According to the obtained results in previous work,[73] the amount of each material put inside the sample holder was around 15 mg for nanoparticles, 40 mg for CBM, and 40 mg for impregnated CBM, to have enough total surface area for sorption. The isotherms were fitted with the Langmuir model, which considers monolayer adsorption of the adsorbate on adsorbent surfaces. The model is described by Equation 1.

$$N_{ads} = \frac{N_{\max} K_L C_e}{1 + K_L C_e} \quad (1)$$

where N_{ads} (mmol g^{-1}) and $N_{\max}$ (mmol g^{-1}) represent the sorbed amount and sorption capacity at equilibrium pressure. K_H represents the sorption equilibrium Langmuir constant, and C_e represents the equilibrium concentration of the asphaltenes in the supernatant.

Results and discussion

Size and morphology.

Table 1 presents the impregnation amount of urea and amine on the synthesized RSi. The results indicate that nanoparticles were successfully impregnated via the incipient wetness technique obtaining close values between experimental and theoretical calculations.

Table 1. The ratio of urea and amine dosage, hydrodynamic diameter (D_p50) of the synthesized nanomaterials

Sample	N-source	Theoretical impregnation (wt.%)	Experimental impregnation (wt.%)
RSi	-	-	-
RSi-U1	Urea	1%	0.98%

RSi-U3	Urea	3%	3.12%
RSi-U5	Urea	5%	5.02%
RSi-DE1	Diethylamine	1%	1.12%
RSi-DE3	Diethylamine	3%	3.01%
RSi-DE5	Diethylamine	5%	5.10%
RSi-TE1	Triethylamine	1%	0.99%
RSi-TE3	Triethylamine	3%	2.98%
RSi-TE5	Triethylamine	5%	4.96%
RSi-EM1	Ethylenediamine	1%	1.03%
RSi-EM3	Ethylenediamine	3%	2.94%
RSi-EM5	Ethylenediamine	5%	5.03%

The morphology and size distribution of nanomaterials obtained from rice husk is presented in Figure 4 for a) Ethylenediamine-EM, b) Diethylamine-DE, c) Triethylamine-TE, and d) Urea-U. The Figure shows that a silica network is formed by nearly spherical particles with different degrees of fusion. The system does not change the structure after active phase inclusion; that is, after doping with the different amines and urea, a similar structure is obtained. The particle size obtained by SEM analysis for non-doped silica was 40 nm.

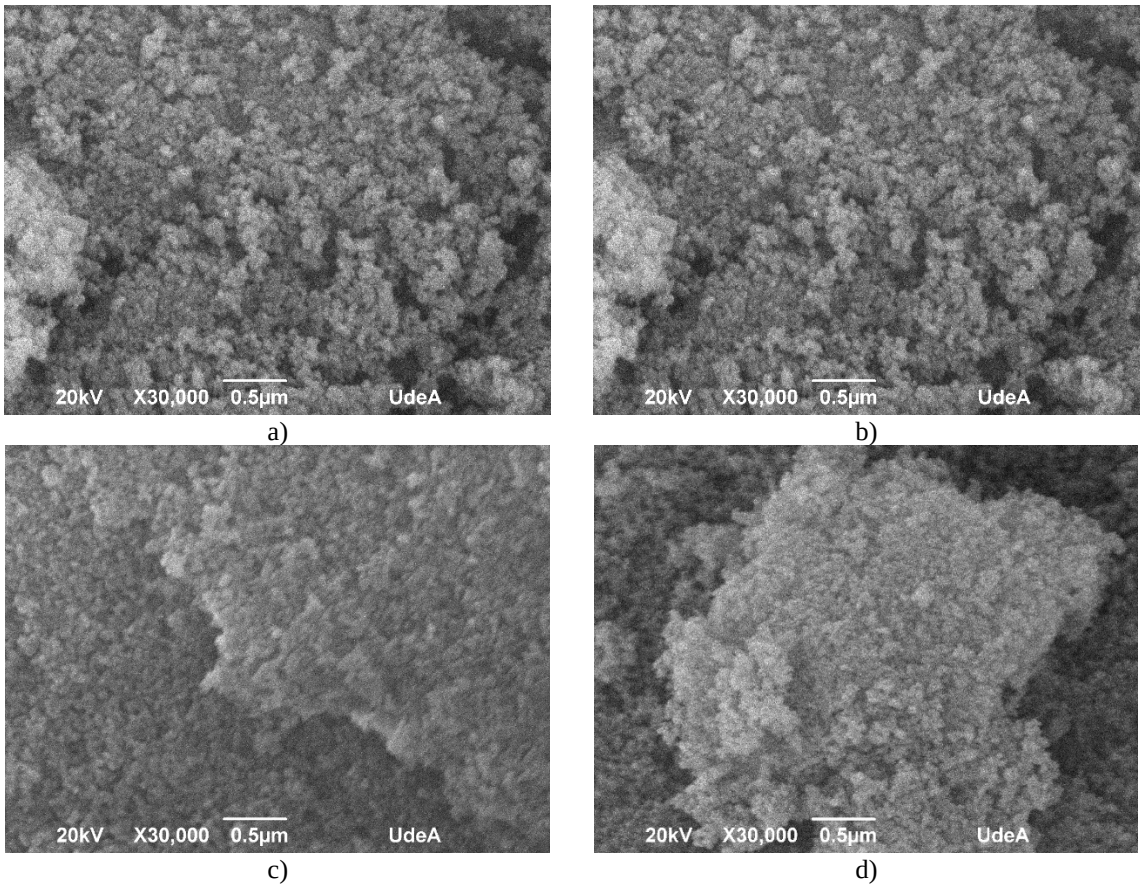

Figure 4. Scanning electron microscopy images of silica doped with 3 wt.% of N-sourced including a) Ethylenediamine-EM, b) Diethylamine-DE, c) Triethylamine-TE, and d) Urea-U.

The size was also analyzed by DLS and the results are shown in Figure 5a. The hydrodynamic diameter of functionalized materials was obtained for particles in water (at pH 5.8). The results show that the average silica nanoparticle diameter increased from 40 nm to at least 90 nm because of the loading with the urea and amine group, which can be attributed to the formation of a thick layer on the surface of the silica nanoparticles. The mean particle size increased in the doping amount order 1 wt.% < 3 wt.% < 5 wt.% for all N-sources used. According to the loading amount of amino functional groups on the surface, they could interact between them,

increasing the size. This result agrees with the report by Hurtado et al.[74], who state that a higher amount of molecules coating the surface of the nanoparticles increases its hydrodynamic diameter.

Regarding the type of amine molecules, considering the same loading amount, the trend increased in order RSi-TE > RSi-U > RSi-DE > RSi-EM; the structure of amine molecules explains these results. The primary amine (EM) exhibits the smallest particle size among the three amino groups. The steric hindrance effect in triethylamine and diethylamine decreases the ability of the amine to position itself in an orderly manner on the surface of the silica nanoparticle, thus, leading to an increase in the average diameter of nanoparticles.

Figure 5b-c summarizes the surface area (S_{BET}) and total surface acidity (TPD-NH_3) values for the synthesized and modified nanoparticles. The RSi presents a total acidity of 100 μmol g^{-1}. Once the RSi is doped with the different N-groups, the acidity decreased. As higher the doped amount, as lower the total acidity. Based on these results, it is expected that Si-OH functional groups are responsible for the NH_3 adsorption; however, the functionalization favors a basic character according to functionalized agent,[61, 75, 76] which modifies the trend of acidity.

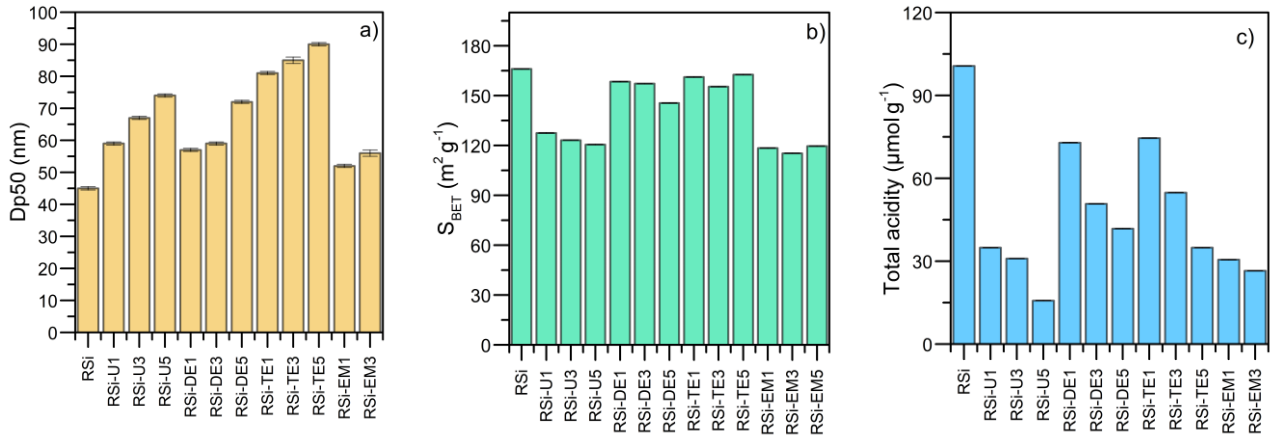

Figure 5. a) Hydrodynamic diameter, b) Surface area (S_{BET}) and c) total surface acidity values of the synthesized nanoparticles

RSi nanoparticles exhibit the highest BET surface area of 166 m^2 g^{-1}. However, the surface modification process decreases the superficial area in the order: RSi-TE< RSi-DE< RSi-U < RSi-EM, respectively. The decrease is described by the fact that the ligands occupy part of the surface of the RSi, reducing the effective surface area.[45] Also, it is observed that this property increases with the decrease of the silica nanoparticle size. For this reason, nanoparticles with a smaller particle size (EM) have a larger surface area.[77]

Interestingly, the results obtained show that the functionalizing agent can change the surface properties of the nanomaterials. The presence of the amines reduces the acidic character of the samples as well as reduces the surface area as is expected.[44] Both properties are reduced with the increase of the N groups (amount of doping source). Interestingly, the total acidity modification follows the same trend that the surface area. These results agree well with those reported by Taborda et al.[78] and Hurtado et al.[79]. This trend is observed for materials modified with nitrogen agents, which favor a basic character relating to changes in the nanoparticle active sites after H_3O^+ deposition.

According to the results shown in Table 2. the total acidity trend of the samples is affected by: (i) the different amino types evaluated as a potential source of active sites on the surface of silica nanoparticles and (ii) the amine coating onto the samples. In this sense, regarding the source of basic sites, the trend of the samples follows the order RSi-EM > RSi-U > RSi-DE > RSi-TE. This trend could be explained due to a higher degree of substitution of alkyl groups by alkoxide groups in the synthesis of RSi-EM and RSi-U nanoparticles compared to RSi-DE and RSi-TE.[77]

Moreover, the amine coating increased the basicity of the silica nanoparticles among all ligands used as surface modifying agents. The trend observed increased in the order 1 wt.% < 3 wt.% < 5 wt%, which could be due to the contribution of the basic amino groups present on the impregnated silica nanoparticles, the higher amount of the impregnated ratio dosage of amines increases the nitrogen content of the samples.[80]

The RSi and amine-functionalized samples are characterized using FT-IR spectroscopy in the mid-infrared region ranging from 450 cm^{-1} to 4500 cm^{-1}. Figures S1-S4 shows the FT-IR spectra of RSi-DE, RSi-TE, RSi-EM, and RSi-U, respectively. The spectra of pure silica materials are also included for comparison to confirm the functionalization of the silica by the amino groups.

The broad absorption band centered between 2580 cm^{-1} and 3460 cm^{-1} is due to the H-bonded silanol groups (Si-OH), and the peak at 1859 cm^{-1} is associated with the Si-O-$Si_{overtones}$. The peak at 1618 cm^{-1} is due to the bending vibration of H-O-H, and the vibration mode at 478 cm^{-1} represents the Si-O bond. The small peaks at 1056 cm^{-1} and 808 cm^{-1} are associated with the symmetric and asymmetric bending and stretching vibration of Si-O-Si linkages.[47, 81]

The amine impregnated samples exhibit similar behavior with three bands at 1051 cm^{-1}, 958 cm^{-1}, and 798 cm^{-1} due to the bending vibration and the symmetric and asymmetric stretching vibration of Si-O-Si.[82] The band observed at 1707 cm^{-1} is related to the water molecules adsorbed on the surface of the silica structure.[83]

Specific differences were found in FTIR spectra for each doped phase. For RSi doped with diethylamine the peak centered at ~3435 cm^{-1} attributed to -OH stretching and N-H stretching in DE became sharp. The peak band observed at 1625 cm^{-1} exhibit the characteristic absorption peak of secondary amines -N-(R)H.[47] In contrast, triethylamine functionalized samples displayed wider bands at 2885 cm^{-1} and 2923 cm^{-1} associated with the symmetric and asymmetric stretching of -CH_2-.The peaks at 1332 cm^{-1} and 1485 cm^{-1} are the deformation swing absorption of the CH bond. The band at 1583 cm^{-1} originated from the rocking vibration absorption band of the NH, and the bands at 2958-3687 cm^{-1} are related to the stretching swing of NH.[84, 85]

For ethylenediamine functionalized samples. the peaks observed at 1517 cm^{-1} and 1462 cm^{-1} are related to N-H_2 vibration of the primary amine presence in RSi-EM impregnated samples. The bands observed at ~3367 cm^{-1} and 3321 cm^{-1} are related to the asymmetric and symmetric vibrations of NH_2. The presence of weak bands at 1618 cm^{-1} indicated NH_2 and NH_3 bands in the EM impregnated samples.[86] Finally, in urea systems, the typical vibrations attributed to the stretching and bending vibration of the N-H groups appeared at 1554 and 3325 cm^{-1}. Moreover, the appearance of the absorption band at 1679 cm^{-1} is assigned to the amide C=O stretching of urea impregnated on the surface of RSi-U nanoparticles.

XPS analysis provides information about the chemical composition and electronic structures of the elements present on a surface and in-depth and the results are summarized in Table 3. The XPS technique monitors the electron binding energy of elements within a few nanometers of the particle surfaces. The investigation of XPS for SiO_2 and N-doped SiO_2 samples was examined for three areas of the XPS spectrum, the Si_{2p} region near 103 eV, the O_{1s} region near 530 eV and the N_{1s} region near 400 eV. A pair of Si_{2p} peaks is located at 102.3 eV and 103.5 eV, corresponding to the Si-O-Si and Si-OH signals of silicon oxide.[87] Each sample presents different percentages of both groups. The Si-OH concentration was higher than Si-O-Si group in all the samples. Comparing the N-source doping mass fraction, the Si-OH decreased by 1 wt.% > 3 wt.% < 5 wt.%. This result indicates that nitrogen is anchored mainly to hydroxyl groups of the SiO_2 nanoparticles. Additionally, at a fixed doping mass fraction, the Si-OH groups were similar regarding the N-source, and that is, Si-OH groups were similar for TE, DE, U, and EM. Details of the results are summarized in Table 3. Similarly, from the O_{1s} spectra of silica nanoparticles without N doped, the deconvoluted spectrum at 533.2 eV is from the SiO_2. The Si/O ratio was similar for all samples (0.5), which agrees well with the silicon structure. However, an additional peak for N-doped SiO_2 appears at 531.7 eV, which is associated with Si-O-N bonds.[88]

The N1s spectrum exhibits two peaks at ~399 eV and ~401.6 eV for the systems doped with EM and U. The first peak accounts for species Si-$((NH_2)C_2H_4)_2$ and Si- $((NH_2)CO)_2$ in RSi-EM and RSi-U, respectively. This BE assignment is consistent with the binding energies of primary/secondary amines (398.9 eV). The second peak is commonly associated with the datively bonded species. In the case of TE- and DE-doped SiO_2, there is one peak close to 399 eV, which may correspond to contributions such as NH_x, NO_x, and NHOH. In the case of the TE and DE, the peak is associated with NH_x structures.

Table 3. Chemical surface composition of silica doped with different loads of N-sourced including Urea-U, Ethylenediamine-EM, Triethylamine-TE, and Diethylamine-DE, determined by XPS.

Sample	Si_{XPS} (%)	O_{XPS} (%)	N_{XPS} (%)	Si-OH (%)	Si-O-Si (%)	Si-O-N (%)	NH_x (%)	Si-NH_x (%)
RSi	33.4	66.6	-	61.2	38.8	-	-	-
RSiU1	33.80	66.1902	0.0098	58.6	41.4	4.5	88.4	11.6
RSiU3	31.30	68.6688	0.0312	58.1	41.9	5.6	85.2	14.8
RSiU5	32.90	67.0498	0.0502	57.3	42.7	8.2	80.4	19.6
RSiDE1	33.50	66.4888	0.0112	60.5	39.5	3.3	100.0	-
RSiDE3	33.30	66.6699	0.0301	60.2	39.8	4.5	100.0	-
RSiDE5	33.20	66.749	0.0510	58.3	41.7	7.7	100.0	-
RSiTE1	33.00	66.9901	0.0099	61.0	39.0	4.4	100	-
RSiTE3	32.40	67.5702	0.0298	60.2	39.8	5.1	100	-
RSiTE5	33.50	66.4504	0.0496	59.1	40.9	7.9	100	-
RSiEM1	32.80	67.1897	0.0103	58.0	42.0	4.7	90.1	9.9
RSiEM3	33.10	66.8706	0.0294	57.3	42.7	6.0	86.2	13.8
RSiEM5	33.60	66.3497	0.0503	56.8	43.2	8.5	83.4	16.6

CO_2 sorption analysis

***CO_2 sorption isotherms on RSi and doped RSi nanoparticles*.** RSi and doped RSi nanoparticles were tested as sorbents for constructing CO_2 sorption isotherms. Figure 6 presents the experimental sorption profiles for RSi and doped silica nanomaterials at 25 °C for pressures up to 3 MPa, and the fit with the Langmuir model. Sorption isotherms of CO_2 obtained for all materials show a type I

behavior according to the IUPAC (International Union of Pure and Applied Chemistry) classification,[89] where it is possible to observe the sorbed amount of CO_2 increases as the absolute pressure increases. The CO_2 uptake follows an increasing trend as pressure increases from 0 to 1.5 MPa and then, between 1.5 MPa and 3.0 MPa, the amount sorbed show a tendency towards stabilization. Overall, the affinity between silanol groups and CO_2 molecules is high, which explains the sorption profile obtained.[90]

RSi capture around 3 mmol CO_2 per gram of the material at equilibrium pressure. Once RSi nanoparticles are coated with urea and amine groups, the CO_2 adsorption amount at the equilibrium and affinity are increased by the presence of functional groups that strongly interact with CO_2 and favor both the physical and chemical sorption processes.[91, 92]

These results agree with the expected acid-base interactions between acidic CO_2 gas molecules and doping agents. Tables S1 to S4 show the Langmuir parameters for the sorption isotherms of RSi and the surface modifications with RSi-EM, RSi-DE, RSi-TE and RSi-U. Values of N_{max} are in the range of 3.9 to 5.9 mmol CO_2 per gram of RSi nanoparticles, increasing with the doped agents, being the best results for the case of EM3. In the same way, the concept of sorption energy related to Langmuir constant K_H has slight changes for each case having a trend of decrease as the sorption capacity of nanomaterials increases.

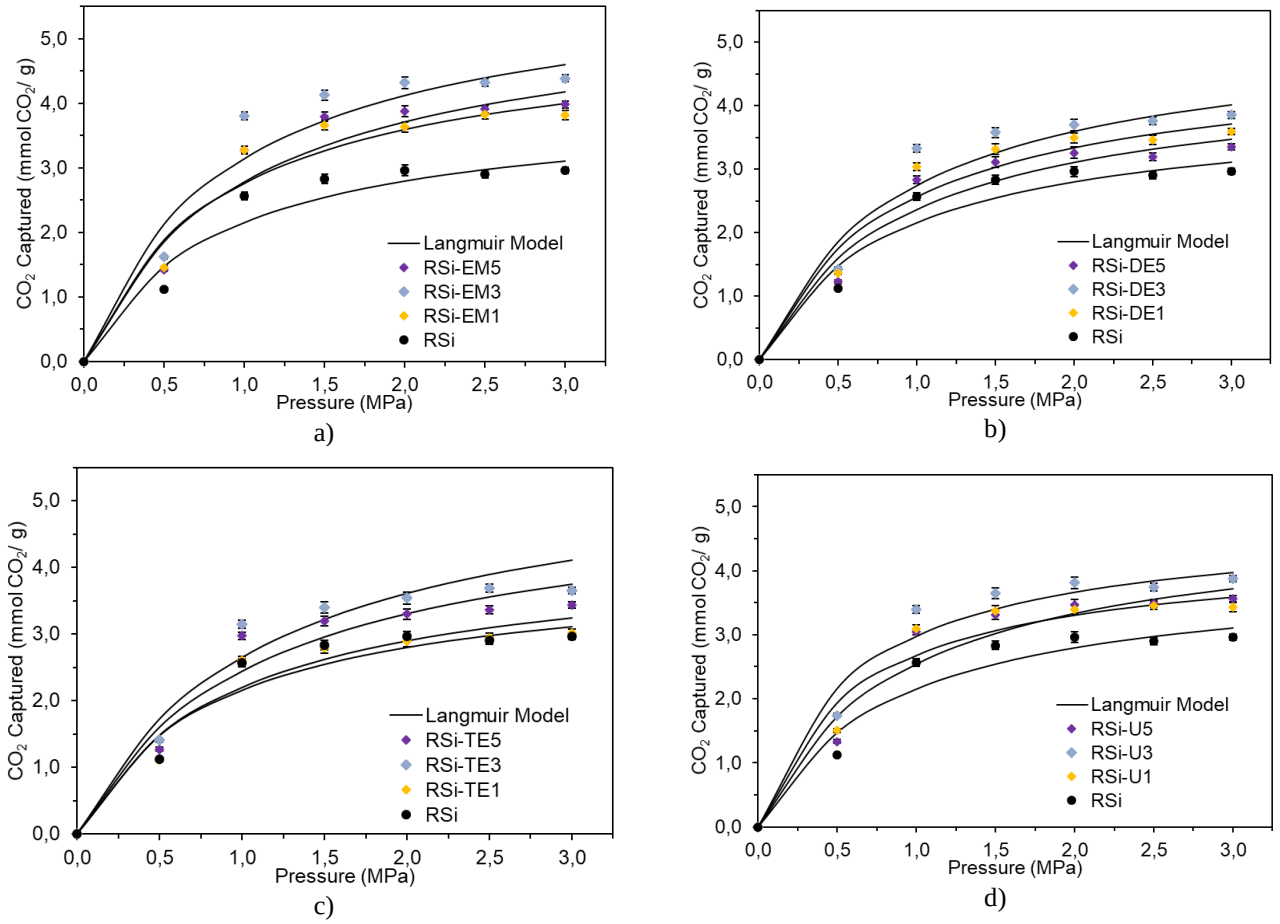

Figure 6. Sorption isotherms of CO_2 at high pressure of RSi and different silica-doped agents. a) RSi-EM, b) RSi-DE, c) RSi-TE and d) RSi-U. The black lines are the Langmuir fit model, and the symbols are the experimental data.

According to Figure 6, for amine-impregnated RSi samples, the sorption performance of RSi changes with the amount of amine and urea loading in terms of the number of amines per total weight of the material.[93] The results obtained in the sorption isotherms are explained by the number of protons combined with nitrogen; therefore, the primary amine group presents the highest reaction rate towards CO_2 than the secondary amine group and even lower for tertiary amines.[44] This happens depending on the nature and structure of the amines, therefore, providing different affinities for an acid gas such as CO_2.[94] Among three ligands used, ethylenediamine presents an accessible N lone pair for interaction with CO_2.[95]

CO_2 sorption analysis on EM-functionalized RSi. Figure 6(a) shows the effect of 1-5 wt.% EM loading on pristine RSi for CO_2 sorption capacity. Among the RSi-EM-impregnated samples of this work, CO_2 uptake of sample RSi-EM3 was found to be maximum (4.39 mmol g^{-1} at 25°C and 3 MPa) due to the presence of many amine functionalities as CO_2 affinity sites. The further increase in the weight percent of EM (5 wt.%) decreases the CO_2 capacity to 3.85 mmol g^{-1} at 25°C and 3 MPa. This result may suggest that the 5 wt.% provokes lower dispersions on the silica surface, reducing its interactions with CO_2.

The result manifests that the amine group can enhance the interaction between CO_2 and the silica for loadings close to 3 wt.%; however, for higher loadings (5 wt.%), the complete filling of pores by amine molecules and excessive coating of ethylenediamine over the silica surface will increase the diffusion resistance of CO_2 molecules to active amine sites and decrease its sorption due to channel blocking.[86]

Different mechanisms can govern the interaction of CO_2 with ethylenediamine. The primary amine can react directly with CO_2 to produce carbamates by forming zwitterionic intermediates.[96] The mechanism for carbamate formation from the reaction of CO_2 with a primary amine is depicted in Figure 7. The first step proceeds with the lone pair on the amine attacking the carbon from CO_2 to form the zwitterion. The free base then deprotonates the zwitterion to form the carbamate.

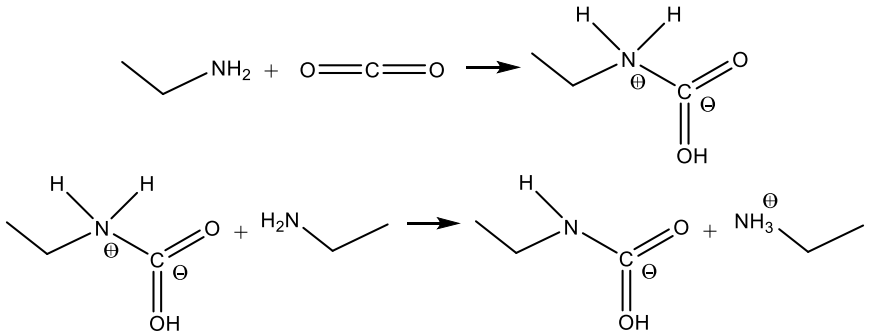

Figure 7. The mechanism for the reaction of CO_2 with a primary amine.

CO_2 sorption analysis on DE-functionalized RSi. RSi was also functionalized with 1, 3, and 5 wt.% of DE to study the impact of secondary amine on CO_2 sorption. CO_2 sorption isotherms of RSi-DE at a temperature of 25°C and 0-3 MPa are shown in Figure 6(b) RSi-DE3 shows a maximum CO_2 sorption capacity of 3.69 mmol g^{-1}, which is lower than RSi-EM3 (4.39 mmol g^{-1}).
Considering Figure 6(b), the result shows a lower CO_2 capture capacity and a decrease in initial CO_2 uptake compared to RSi-EM3; the possible reason may be because of steric hindrance. Compared to the EM molecule, DE has a larger molecular structure where two alkyl groups are linked to the central "N" atom.[97] Moreover, the pronounced effect of a steric hindrance has resulted in the decrease of CO_2 sorption performance in the order of RSi-DE3>RSi-DE1>RSi-DE5. The sorption mechanism of CO_2 on DE is depicted in Figure 8.

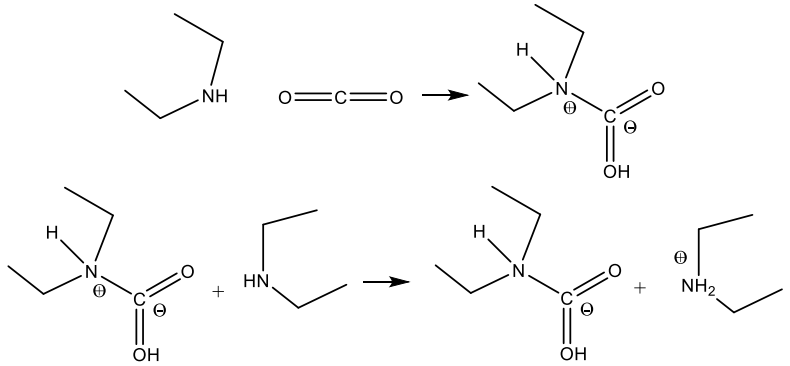

Figure 8. The mechanism for the reaction of CO_2 with a secondary amine.

The carbamate is a CO_2-induced product of secondary amines with a neighboring amine. CO_2 is bonded to secondary amines as a carbamic acid and converted to carbamate by adjacent amine.[98] Although secondary amines are basic as primary amines and exhibit high reactivity to CO_2. Steric hindrance reduces its ability to chemisorb to form a carbamate, resulting in freer amine for CO_2 sorption.[99]

CO_2 sorption analysis on TE-functionalized RSi. To study the effect of tertiary amine on RSi for CO_2 sorption. RSi was functionalized with 1-3 wt.% triethylamine (TE). CO_2 sorption isotherms of RSi-TE at a temperature of 25°C and up to 3 MPa is

shown in Figure 6(c) RSi-TE3 shows a maximum CO_2 sorption capacity of 3.65 mmol g^{-1}, which is lower than both RSi-EM3 and RSi-DE3, but slightly higher than that observed using pristine RSi.

Three alkyl groups could explain the lower CO_2 sorption on the central "N" atom, resulting in steric hindrance for interaction with CO_2 molecules.[97] This steric hindrance effect phenomenon causes a CO_2 molecule to be sorbed by one amino group in the middle of a molecular chain, causing difficulty for other amino groups to approach CO_2 molecules.[100] It also could be explained because tertiary amine groups cannot offer free protons to react with CO_2. These results imply that the type and structure of amine molecules strongly influence the CO_2 sorption capacity of the amine functionalized RSi sorbent.

For a tertiary amine, such as triethylamine, instead of reacting with CO_2, the reaction mechanism could be due to electrostatic attraction and Van der Walls forces, or tertiary amines could catalyze the formation of bicarbonate through a different mechanism.[101] Figure 9 shows the mechanism involving the base-catalyzed hydration of CO_2. [102, 103] In the first step, the tertiary amine dissociates H_2O to form a quaternary cationic species and OH^-. Hydroxide ion then attacks CO_2 to form the bicarbonate anion. The last step is the ionic association of the protonated amine and bicarbonate.

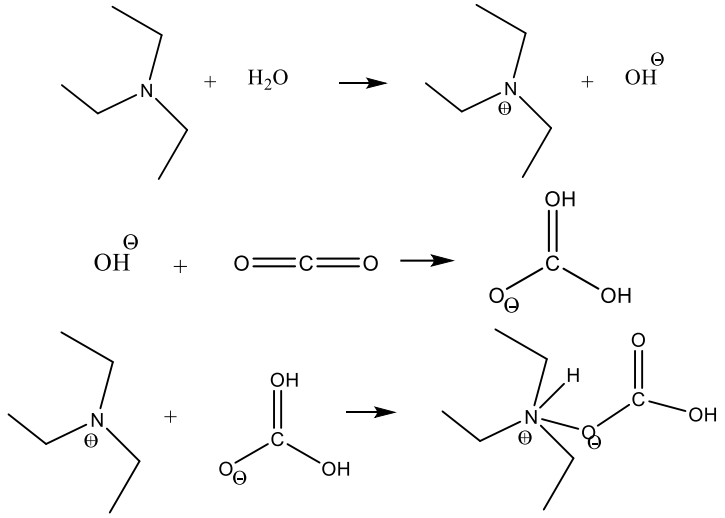

Figure 9. The mechanism for the reaction of CO_2 with a tertiary amine.

CO_2 sorption analysis on U-functionalized RSi. Figure 6(d) shows that the CO_2 uptake on RSi-U3 is the highest (i.e.,3.8 mmol g^{-1}), that on RSi-U5 is the second (i.e.,3.6 mmol g^{-1}), and that on RSi-U1 is the lowest (i.e.,3.4 mmol g^{-1}). Urea is characterized by the presence of a carboxylic group in its chemical structure. As a result, the urea's basicity is lower than the basicity of the ethylenediamine, leading to a lower uptake of CO_2.

The formation mechanism between urea and silica nanoparticles by non-covalent interaction is given in Figure 10. The dashed lines represent the hydrogen bonds between silica and urea. A urea layer can be formed on the particle surface of silica due to the hydrogen bond interaction between the amino group of urea and hydroxyl groups on silica. [104]

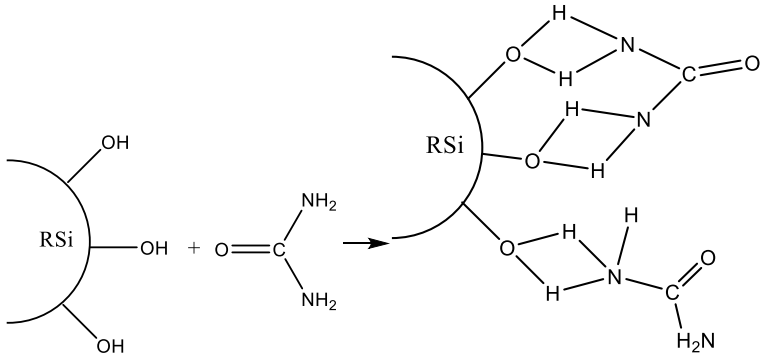

Figure 10. The formation mechanism of urea-modified silica nanoparticles

CO_2 can act as a Lewis acid and interact with electron donors through partial charge transfer to the carbon atom. Urea-functionalized silica nanoparticles containing carbonyl and amine groups are considered potential electron donors (Lewis's base) due to the lone pair electrons on the oxygen atoms.[105] Therefore, the interaction between CO_2 and the RSi-U is due to Lewis acid- Lewis base interaction.

CO_2 is chemisorbed at the primary (NH_2) and the secondary (NH) amine functions in urea. The free -NH_2 could serve as a Lewis basic site.

The individual CO_2 sorption capacity of nanoparticles increased in the order RSi-TE<RSi-DE<RSi-U<RSi-EM. The uptake CO_2 amount is higher for the primary amine, with a difference of 0.71 mmol g^{-1} (at 25°C) reached at the maximum pressure (3.0 MPa). Some properties were higher in the RSi doped with EM, like the total acidity, the surface area, the content of Si-O-N, NH_x, or Si-NH_x groups, and the total nitrogen content normalized by the surface area of the nanoparticles. Some of these properties are correlated with the CO_2 sorption capacity of the nanoparticles and are shown in Figure 11. For example, the lower the total acidity, the greater functional groups are expected to be exposed to form specific ligands (Si-O-N), which favors the sorption process.[77] This result also agrees with the CO_2 reaction mechanisms presented above, the steric hindrance associated with the alkyl linked to the central N atom in both RSi-DE and RSi-TE.

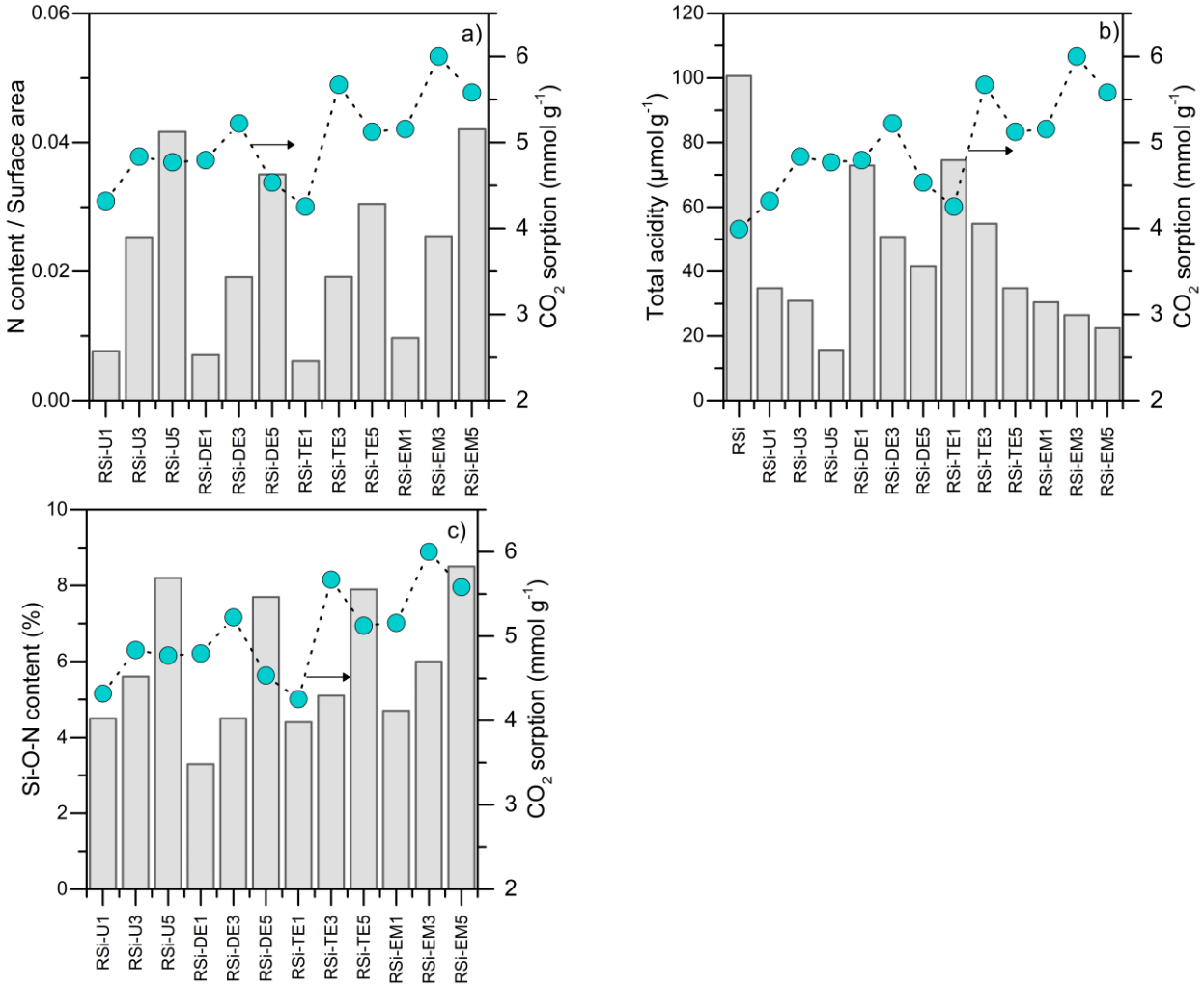

Figure 11. CO_2 sorption as a function of a) nitrogen content normalized by surface area, total acidity, and Si-O-N content of synthesized RSi nanoparticles.

On the other hand, although there are two amino groups in EM and U chemical structures, these groups are joined by a carbonyl (C=O) functional group in the U samples, reducing their reactivity compared to EM`s amino groups connecting to a hydrocarbon chain. Hence, the CO_2 sorption capacity decreases the sorption capacity: RSi-TE<RSi-DE<RSi-U<RSi-EM. Also, while comparing the effect of amine loading on all surface modifiers, the addition of 1, 3, and 5 wt.% amine to silica nanoparticles leads to an increase in the average CO_2 sorption capacity; however, a further increase in the amine loading to 5 wt.% will cause steric hindrance and agglomeration of particles, which have a negative impact on the diffusion of CO_2 reducing the CO_2 sorption capacity due to blockage of the porous structure (i.e., 5 wt.% < 1 wt.% < 3 wt.%).[46, 106] Therefore, the CO_2 maximum sorption capacity was similarly obtained for all 3 wt.% N-source impregnated silica systems, increasing as RSi-TE3<RSi-DE3<RSi-U3<RSi-EM3. These systems presented the highest sorption performance and were evaluated for selective CO_2 sorption from flue gas streams.

CO_2 sorption from flue gas stream on CBM. Figure 12 presents the adsorption isotherms for CBM and doped CBM with 10 wt.% and 20 wt.% of RSi at 50 °C for pressures up to 3.0 MPa for CO_2 (panel a) and N_2 (panel b) and the fit with the Langmuir model. The adsorption isotherm of CO_2 on CBM and CBM-10RSi follows the Ib-type behavior concerning the IUPAC classification.[63, 107] These types of isotherms are characterized by the increase of the adsorbed amount of CO_2 as the absolute pressure increases. The CO_2 maximum adsorption amount on CBM was close to 0.05 mmol g^{-1}. Once the system is doped with 10 and 20 wt.% of silica, the adsorption amount at the highest pressure increases to 0.53 and 0.56 mmol g^{-1}, respectively. This increase represents more than a 1000% improvement in the adsorption properties of the CBM for both impregnations. The weak interactions between CBM and CO_2 could be associated with the high content of inorganic carbon on CBM. Busch et al.[108] confirmed that that organic matter controls the CO_2 storage capacity on CBM, and the inorganic carbon accommodates a small additional CO_2 sorption capacity At pressures higher than 0.2 MPa, the amount adsorbed increases gradually. The Henry region is found for pressures < 0.2 MPa, showing a higher affinity for the CO_2 in the doped system than virgin CBM. Meanwhile, the nitrogen adsorption is null regarding the CO_2 adsorption for both systems. This behavior is typical for sieve samples where the materials do not have an affinity for nitrogen.

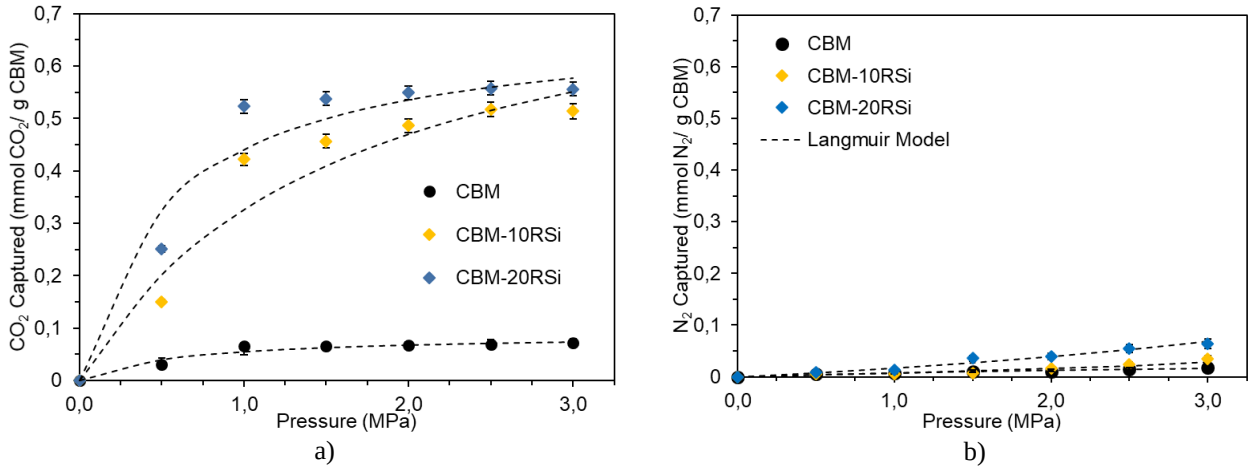

a) b)

Figure 12. Adsorption isotherms of a) CO_2 and b) N_2 at high pressure of CBM and CBM doped with 10 and 20 wt.% of silica nanoparticles (RSi). The dotted lines are the Langmuir fit model, and the symbols are the experimental data.

Figures 13 and 14 show the CO_2 (panel a) and N_2 (panel b) sorption isotherms over the CBM impregnated with 10 wt.% and 20 wt.% of the best systems obtained in the previous section, where individual CO_2 sorption was evaluated. The selected systems are RSiEM3, RSiTE3, RSiDE3, and RSiU3. The evaluation of CO_2 sorption in the flue gas streams indicates that the sorption capacity is considerably higher for the doped CBM than the sample without surface modification.

From panel a, it is deduced that the CO_2 sorption amount increased in the order CBM-10RSiTE3 < CBM-10RSiDE3 < CBM-10RSiU3 < CBM-10RSiEM3, which agrees well with the discussion presented in the previous section. While the maximum amount of sorbed CO_2 for CBM-10RSiEM3 was almost 0.72 mmol g^{-1}, it was approximately 0.65 mmol g^{-1} for CBM-10RSiU3, 0.59 mmol g^{-1} for CBM-10RSiDE3, 0.53 mmol g^{-1} for CBM-10RSiTE3, and 0.46 mmol g^{-1} for CBM-10RSi which were all achieved at the maximum pressure (3.0 MPa). The EM system presents two amino groups in its chemical structure, similarly to U, whereas TE and DE only give one amino group, which directly affects the interactions with CO_2. Additionally, in urea, the amino groups are joined to C=O groups, reducing their effectiveness for CO_2 interactions regarding EM structures.

However, regarding CBM, all the systems enhance the sorption capacity. This can be explained by the nanoparticle coming from a biomass by-product precursor in which other components may interact with CO_2 molecules and/or geological media.[73, 109] Moreover, this effect could be related to the CO_2 quadrupole moment, which allows CO_2–CO_2 interaction at high-pressure conditions and surface interactions.[6] Moreover, it should be remarked that the CO_2 sorption capacities reported in the present work are competitive and, in some cases, superior to those found in the literature, including materials with a more complex synthesis process or more stages.[26, 110-112] Similar to the SS, the nitrogen sorption is null regarding the CO_2 sorption for all systems evaluated, highlighting the selectivity of the synthesized materials for CO_2 sorption in flue gas currents. Parameters of Langmuir model are showed in Tables S5 to S8 where is observed a trend according to increase of sorption capacity of each sample. Values of N_{max} increasing with the best doped agent EM at dosage of 3%. Besides, the Langmuir constant K_H related to sorption energy show a slight change following a trend of decrease as the sorption capacity of nanomaterials increase. RSME% values maintain less than 10% being evidence of the good fitting between experimental data and theoretical model.

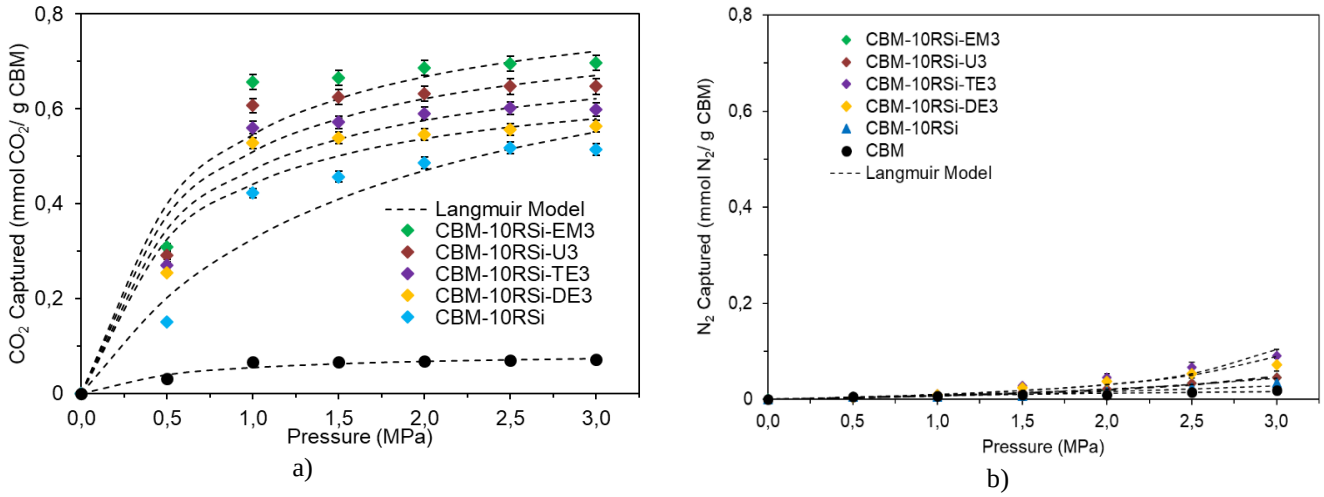

Figure 13. Sorption isotherms of a) CO_2 and b) N_2 at high pressure of CBM and CBM doped with 10 wt.% of silica nanoparticles functionalized with 3 wt.% of the different N-sources (Urea-U, Ethylenediamine-EM, Triethylamine-TE, and Diethylamine-DE). The dotted lines are the Langmuir fit model and the symbols are the experimental data.

Figure 14 shows the results for CBM impregnated with 20 wt.% of nanoparticles. Panel a shows CO_2 sorption isotherms and panel b N_2 sorption isotherm. From panel a, it is deduced that the CO_2 sorption amount increased in the same order than the obtained for 10 wt.%. However, the sorption amount increased once the systems are doped with 20 wt.% regarding 10 wt.%. The maximum amount of sorbed CO_2 for CBM-20RSiEM3, CBM-20RSiU3, CBM-20RSiDE3, CBM-20RSiTE3, and CBM-20RSi was around 0.75 mmol g^{-1}, 0.68 mmol g^{-1}, 0.63 mmol g^{-1}, 0.61 mmol g^{-1}, and 0.56 mmol g^{-1}, respectively.

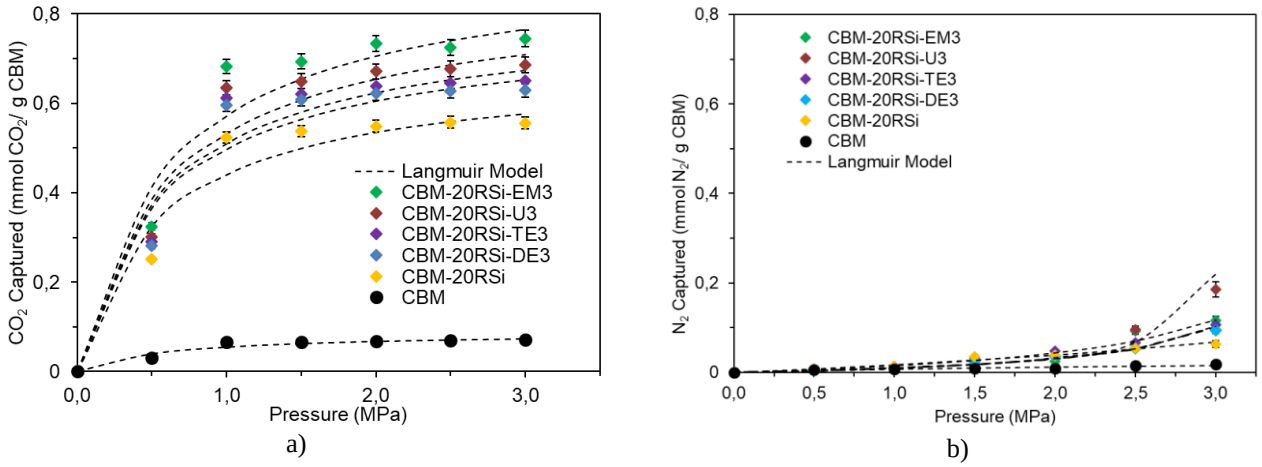

Figure 14. Sorption isotherms of a) CO_2 and b) N_2 at high pressure of CBM and CBM doped with 20 wt.% of silica nanoparticles functionalized with 3 wt.% of the different N-sources (Urea-U, Ethylenediamine-EM, Triethylamine-TE, and Diethylamine-DE). The dotted lines are the Langmuir fit model and the symbols are the experimental data.

Conclusions

This work aimed to assess the potential of carbon sequestration in shallow CBM reservoirs based in nanoparticle inclusion by enhanced sorptive phenomena. To the best of our knowledge, this is the first study using amine-functionalized biomass-derived silica nanoparticles used as a modifying agent to improve the chemical-physical properties of geological media (CBM) to enhance the CO_2 selective sorption in a shallow reservoir in a carbon sorption and storage (CCS) process. The results showed that CO_2 sorption on RSi increases with the N-group coating in the order RSi-DE < RSi-TE < RSi-U < RSi-EM. Although there are two amino groups in EM and U chemical structures, these groups are joined by a carbonyl (C=O) functional group in the U samples, reducing their reactivity

compared to EM`s amino groups connecting to a hydrocarbon chain. Similarly, the steric hindrance associated with the alkyl linked to the central N atom RSi-TE systems favors the greater number of functional groups exposed to form specific ligands that result in higher CO_2 sorption. Also, while comparing the effect of amine loading on all surface modifiers, the addition of 1, 3, and 5 wt.% amine to silica nanoparticles leads to an increase in the average CO_2 sorption capacity; however, a further increase in the amine loading to 5 wt.% will cause agglomeration of particles, which have a negative impact on the diffusion of CO_2 reducing the CO_2 sorption capacity due to blockage of the porous structure. For CBM impregnation, the nanofluid containing 20 wt.% of RSi-EM3 presented the best yield increasing the CO_2 sorption from 0.05 to 0.75 mmol g^{-1}, meaning an increase of more than 1000% in the sorption capacity.

These biomass-derived silica nanomaterials synthesized by a simple process showed high CO_2 selectivity and sorption capacity. The results suggest a competitive CO_2 sorption performance compared to other nanomaterials reported in the literature. Therefore, this research opens an interesting line in the field of biomass-derived nanomaterials for application-enhanced carbon sorption and geological storage (e-CCS).

Acknowledgments

We specifically express our appreciation to the research group Fenómenos de Superficie “Michael Polanyi”. The Universidad Nacional de Colombia jointly supports this study. The authors thank The Royal Academy of Engineering under Collaboration Agreement TSP 2021-100350 for the support provided to develop this study.

References

1. Firdaus, R. M.; Desforges, A.; Mohamed, A. R.; Vigolo, B., Progress in adsorption capacity of nanomaterials for carbon dioxide capture: A comparative study. *Journal of Cleaner Production* **2021,** 328, 129553.
2. Chen, S.; Zhu, M.; Fu, Y.; Huang, Y.; Tao, Z.; Li, W., Using 13X, LiX, and LiPdAgX zeolites for CO2 capture from post-combustion flue gas. *Applied energy* **2017,** 191, 87-98.
3. Change, I. C., Synthesis Report. Contribution of working groups I. *II and III to the fifth assessment report of the intergovernmental panel on climate change* **2014,** 151, (10.1017).
4. Bui, M.; Adjiman, C.; Bardow, A.; Anthony, E.; Boston, A.; Brown, S.; Fennell, P.; Fuss, S.; Galindo, A.; Hackett, L., & Mac Dowell, N.(2018). Carbon capture and storage (CCS): The way forward [10.1039/C7EE02342A]. *Energy & Environmental Science* 11, (5), 1062-1176.
5. Haszeldine, R. S.; Flude, S.; Johnson, G.; Scott, V., Negative emissions technologies and carbon capture and storage to achieve the Paris Agreement commitments. *Philosophical Transactions of the Royal Society A: Mathematical, Physical and Engineering Sciences* **2018,** 376, (2119), 20160447.
6. Gibbins, J.; Chalmers, H., Carbon capture and storage. *Energy policy* **2008,** 36, (12), 4317-4322.
7. Haszeldine, R. S., Carbon capture and storage: how green can black be? *Science* **2009,** 325, (5948), 1647-1652.
8. Philibert, C., Technology penetration and capital stock turnover. Lessons from IEA scenario analysis. **2007**.
9. Change), I. I. P. o. C. *Special Report on Carbon Dioxide Capture and Storage*; Cambridge, UK and

New York, NY, USA, 2005; p 442.
10. Bachu, S. J. I. J. o. G. G. C., Carbon dioxide storage capacity in uneconomic coal beds in Alberta, Canada: Methodology, potential and site identification. **2007,** 1, (3), 374-385.
11. Hildenbrand, A.; Krooss, B. M.; Busch, A.; Gaschnitz, R. J. I. J. o. c. g., Evolution of methane sorption capacity of coal seams as a function of burial history—a case study from the Campine Basin, NE Belgium. **2006,** 66, (3), 179-203.
12. Sarhosis, V.; Hosking, L. J.; Thomas, H. R., Carbon sequestration potential of the South Wales Coalfield. *Environmental Geotechnics* **2016,** 5, (4), 234-246.
13. Mojica, L.; Mariño, J. J. B. d. G., Estado de la exploración y posibilidades de gas asociado al carbón (GAC) en Boyacá (Colombia). **2013,** 35, (2), 31-43.
14. Tewalt, S. J.; Finkelman, R. B.; Torres, I. E.; Simoni, F., World Coal Quality Inventory: Colombia. *US Geological Survey Open File Report* **2006,** 2006, 1241.
15. Harpalani, S.; Prusty, B. K.; Dutta, P., Methane/CO2 sorption modeling for coalbed methane production and CO2 sequestration. *Energy & Fuels* **2006,** 20, (4), 1591-1599.
16. Li, X.; Fang, Z.-m., Current status and technical challenges of CO2 storage in coal seams and enhanced coalbed methane recovery: an overview. *International Journal of Coal Science Technology*

2014, 1, (1), 93-102.

17. Mukherjee, M.; Misra, S., A review of experimental research on Enhanced Coal Bed Methane (ECBM) recovery via CO2 sequestration. *Earth-Science Reviews* **2018,** 179, 392-410.
18. Pham, T.-H.; Lee, B.-K.; Kim, J.; Lee, C.-H., Enhancement of CO2 capture by using synthesized nano-zeolite. *Journal of the Taiwan Institute of Chemical Engineers* **2016,** 64, 220-226.
19. Rajabi, M.; Moradi, O.; Zare, K., Kinetics adsorption study of the ethidium bromide by graphene oxide as adsorbent from aqueous matrices. *International Nano Letters* **2017,** 7, (1), 35-41.
20. Wang, X.; He, T.; Hu, J.; Liu, M. J. E. S. N., The progress of nanomaterials for carbon dioxide capture via the adsorption process. **2021,** 8, (4), 890-912.
21. Saleh, T. A. J. R. a., Nanomaterials and hybrid nanocomposites for CO 2 capture and utilization: environmental and energy sustainability. **2022,** 12, (37), 23869-23888.
22. Creamer, A. E.; Gao, B. J. E. s.; technology, Carbon-based adsorbents for postcombustion CO2 capture: a critical review. **2016,** 50, (14), 7276-7289.
23. Firdaus, R. M.; Desforges, A.; Mohamed, A. R.; Vigolo, B. J. J. o. C. P., Progress in adsorption capacity of nanomaterials for carbon dioxide capture: A comparative study. **2021,** 328, 129553.
24. Rodriguez Acevedo, E.; Cortés, F. B.; Franco, C. A.; Carrasco-Marín, F.; Pérez-Cadenas, A. F.; Fierro, V.; Celzard, A.; Schaefer, S.; Cardona Molina, A. J. M., An enhanced carbon capture and storage Process (e-CCS) applied to shallow reservoirs using nanofluids based on nitrogen-rich carbon Nanospheres. **2019,** 12, (13), 2088.
25. Rodriguez Acevedo, E.; Franco, C. A.; Carrasco-Marín, F.; Pérez-Cadenas, A. F.; Cortés, F. B. J. N., Biomass-Derived Carbon Molecular Sieves Applied to an Enhanced Carbon Capture and Storage Process (e-CCS) for Flue Gas Streams in Shallow Reservoirs. **2020,** 10, (5), 980.
26. Daud, N.; Najib, N., Adsorption of CO2 on ZSM-5 and Cu-MOF at room temperature and low pressure conditions for Carbon Capture and Storage (CCS) application. *Materials Today: Proceedings* **2022**.
27. Kumar, S.; Srivastava, R.; Koh, J., Utilization of zeolites as CO2 capturing agents: Advances and future perspectives. *Journal of CO2 Utilization* **2020,** 41, 101251.
28. Murge, P.; Dinda, S.; Roy, S., Zeolite-based sorbent for CO2 capture: Preparation and performance evaluation. *Langmuir* **2019,** 35, (46), 14751-14760.
29. Abid, H. R.; Rada, Z. H.; Duan, X.; Sun, H.; Wang, S., Enhanced CO2 adsorption and selectivity of CO2/N2 on amino-MIL-53 (Al) synthesized by polar co-solvents. *Energy & Fuels* **2017,** 32, (4), 4502-4510.
30. Su, X.; Bromberg, L.; Martis, V.; Simeon, F.; Huq, A.; Hatton, T. A., Postsynthetic functionalization of Mg-MOF-74 with tetraethylenepentamine: structural characterization and enhanced CO2 adsorption. *ACS applied materials & interfaces* **2017,** 9, (12), 11299-11306.
31. Ding, M.; Flaig, R. W.; Jiang, H.-L.; Yaghi, O. M., Carbon capture and conversion using metal–organic frameworks and MOF-based materials. *Chemical Society Reviews* **2019,** 48, (10), 2783-2828.
32. Ghanbari, T.; Abnisa, F.; Daud, W. M. A. W., A review on production of metal organic frameworks (MOF) for CO2 adsorption. *Science of The Total Environment* **2020,** 707, 135090.
33. Shen, Z.; Cai, Q.; Yin, C.; Xia, Q.; Cheng, J.; Li, X.; Wang, Y., Facile synthesis of silica nanosheets with hierarchical pore structure and their amine-functionalized composite for enhanced CO2 capture. *Chemical Engineering Science* **2020,** 217, 115528.
34. Sánchez-Zambrano, K.; Vilarrasa-García, E.; Maia, D.; Bastos-Neto, M.; Rodríguez-Castellon, E.; Azevedo, D., Adsorption microcalorimetry as a tool in the characterization of amine-grafted mesoporous silicas for CO2 capture. *Adsorption* **2020,** 26, (2), 165-175.
35. Lashaki, M. J.; Sayari, A., CO2 capture using triamine-grafted SBA-15: The impact of the support pore structure. *Chemical Engineering Journal* **2018,** 334, 1260-1269.
36. Li, W.; Yang, H.; Jiang, X.; Liu, Q., Highly selective CO2 adsorption of ZnO based N-doped reduced graphene oxide porous nanomaterial. *Applied Surface Science* **2016,** 360, 143-147.
37. Rao, L.; Liu, S.; Wang, L.; Ma, C.; Wu, J.; An, L.; Hu, X., N-doped porous carbons from low-temperature and single-step sodium amide activation of carbonized water chestnut shell with excellent CO2 capture performance. *Chemical Engineering Journal* **2019,** 359, 428-435.
38. Wang, X.; He, T.; Hu, J.; Liu, M., The progress of nanomaterials for carbon dioxide capture via the adsorption process. *Environmental Science: Nano* **2021,** 8, (4), 890-912.
39. Ren, Y.; Ding, R.; Yue, H.; Tang, S.; Liu, C.; Zhao, J.; Lin, W.; Liang, B., Amine-grafted mesoporous copper silicates as recyclable solid amine sorbents for post-combustion CO2 capture. *Applied energy* **2017,** 198, 250-260.
40. Lee, S. C.; Kim, M. J.; Kwon, Y. M.; Chae, H. J.; Cho, M. S.; Park, Y. K.; Seo, H. M.; Kim, J. C., Novel regenerable solid sorbents based on lithium orthosilicate for carbon dioxide capture at high temperatures. *Separation and Purification Technology* **2019,** 214, 120-127.
41. Li, K.-M.; Jiang, J.-G.; Tian, S.-C.; Chen, X.-J.; Yan, F., Influence of silica types on synthesis and performance of amine–silica hybrid materials used for CO2 capture. *The Journal of Physical Chemistry C* **2014,** 118, (5), 2454-2462.

42. Wu, Y.; Du, H.; Gao, Y.; Liu, X.; Yang, T.; Zhao, L.; Yue, X.; Zhang, S.; Zhang, J., Syntheses of four novel silicate-based nanomaterials from coal gangue for the capture of CO2. *Fuel* **2019,** 258, 116192.
43. Aboudheir, A.; Tontiwachwuthikul, P.; Chakma, A.; Idem, R., Kinetics of the reactive absorption of carbon dioxide in high CO2-loaded, concentrated aqueous monoethanolamine solutions. *Chemical Engineering Science* **2003,** 58, (23-24), 5195-5210.
44. Sayari, A.; Belmabkhout, Y.; Da'na, E., CO2 deactivation of supported amines: does the nature of amine matter? *Langmuir* **2012,** 28, (9), 4241-4247.
45. Cueto-Díaz, E. J.; Suárez-García, F.; Gálvez-Martínez, S.; Valles-González, M. P.; Mateo-Marti, E., CO2 adsorption capacities of amine-functionalized microporous silica nanoparticles. *Reactive and Functional Polymers* **2022,** 170, 105100.
46. Li, X.; Wang, Z.; Liu, Z.; Feng, R.; Song, S.; Huang, J.; Fang, Y., A novel preparation of solid amine sorbents for enhancing CO2 adsorption capacity using alumina-extracted waste. *Energy* **2022,** 248, 123677.
47. Boonpoke, A.; Chiarakorn, S.; Laosiripojana, N.; Chidthaisong, A., Enhancement of carbon dioxide capture by amine-modified rice husk mesoporous material. *Environmental Progress & Sustainable Energy* **2016,** 35, (6), 1716-1723.
48. Ghorbani, F.; Sanati, A. M.; Maleki, M., Production of silica nanoparticles from rice husk as agricultural waste by environmental friendly technique. *Environmental Studies of Persian Gulf* **2015,** 2, (1), 56-65.
49. Montes, D.; Henao, J.; Taborda, E. A.; Gallego, J.; Cortés, F. B.; Franco, C. A., Effect of textural properties and surface chemical nature of silica nanoparticles from different silicon sources on the viscosity reduction of heavy crude oil. *ACS omega* **2020,** 5, (10), 5085-5097.
50. Franco, C. A.; Cortés, F. B.; Nassar, N. N., Adsorptive removal of oil spill from oil-in-fresh water emulsions by hydrophobic alumina nanoparticles functionalized with petroleum vacuum residue. *Journal of colloid and interface science* **2014,** 425, 168-177.
51. Leofanti, G.; Padovan, M.; Tozzola, G.; Venturelli, B., Surface area and pore texture of catalysts. *Catalysis Today* **1998,** 41, (1), 207-219.
52. Brunauer, S.; Emmett, P. H.; Teller, E., Adsorption of gases in multimolecular layers. *J. Am. Chem. Soc* **1938,** 60, (2), 309-319.
53. Brunauer, S.; Emmett, P. H.; Teller, E., Adsorption of gases in multimolecular layers. *Journal of the American Chemical Society* **1938,** 60, (2), 309-319.
54. Partyka, S.; Rouquerol, F.; Rouquerol, J., Calorimetric determination of surface areas: Possibilities of a modified Harkins and Jura procedure. *Journal of Colloid and Interface Science* **1979,** 68, (1), 21-31.
55. Harkins, W. D.; Jura, G., An adsorption method for the determination of the area of a solid without the assumption of a molecular area, and the area occupied by nitrogen molecules on the surfaces of solids. *The Journal of Chemical Physics* **1943,** 11, (9), 431-432.
56. Gregg, S. J.; Sing, K. S. W.; Salzberg, H., Adsorption surface area and porosity. *Journal of The electrochemical society* **1967,** 114, (11), 279Ca.
57. Geography, U. D. o., SediGraph particle size analysis. In UCL: 2014.
58. Franco, C. A.; Lozano, M. M.; Acevedo, S.; Nassar, N. N.; Cortés, F. B., Effects of Resin I on Asphaltene Adsorption onto Nanoparticles: A Novel Method for Obtaining Asphaltenes/Resin Isotherms. *Energy & Fuels* **2015,** 30, (1), 264-272.
59. López, D.; Giraldo, L. J.; Salazar, J. P.; Zapata, D. M.; Ortega, D. C.; Franco, C. A.; Cortés, F. B. J. C., Metal Oxide Nanoparticles Supported on Macro-Mesoporous Aluminosilicates for Catalytic Steam Gasification of Heavy Oil Fractions for On-Site Upgrading. **2017,** 7, (11), 319.
60. Kuśtrowski, P.; Chmielarz, L.; Bożek, E.; Sawalha, M.; Roessner, F., Acidity and basicity of hydrotalcite derived mixed Mg–Al oxides studied by test reaction of MBOH conversion and temperature programmed desorption of NH 3 and CO 2. *Materials Research Bulletin* **2004,** 39, (2), 263-281.
61. AlSawalha, M.; Roessner, F.; Novikova, L.; Bel'chinskaya, L., Acidity of different Jordanian Clays characterized by TPD-NH3 and MBOH Conversion. *World Acad. Sci. Eng. Technol* **2011,** 5, 7-29.
62. Al-Oweini, R.; El-Rassy, H., Synthesis and characterization by FTIR spectroscopy of silica aerogels prepared using several Si (OR) 4 and R″ Si (OR′) 3 precursors. *Journal of Molecular Structure* **2009,** 919, (1), 140-145.
63. Rodriguez Acevedo, E.; Franco, C. A.; Carrasco-Marín, F.; Pérez-Cadenas, A. F.; Cortés, F. B., Biomass-Derived Carbon Molecular Sieves Applied to an Enhanced Carbon Capture and Storage Process (e-CCS) for Flue Gas Streams in Shallow Reservoirs. *Nanomaterials* **2020,** 10, (5), 980.
64. Werner, M.; Verduyn, M.; van Mossel, G.; Mazzotti, M. J. E. P., Direct flue gas CO2 mineralization using activated serpentine: Exploring the reaction kinetics by experiments and population balance modelling. **2011,** 4, 2043-2049.
65. Medina, O. E.; Gallego, J.; Rodríguez, E.; Franco, C. A.; Cortés, F. B. J. E.; Fuels, Effect of pressure on the oxidation kinetics of Asphaltenes. **2019,** 33, (11), 10734-10744.
66. Medina, O. E.; Gallego, J.; Acevedo, S.; Riazi, M.; Ocampo-Pérez, R.; Cortés, F. B.; Franco, C. A., Catalytic Conversion of n-C7 Asphaltenes and Resins II into Hydrogen Using CeO2-Based Nanocatalysts. *Nanomaterials* **2021,** 11, (5), 1301.

67. Medina, O. E.; Gallego, J.; Pérez-Cadenas, A. F.; Carrasco-Marín, F.; Cortés, F. B.; Franco, C. A., Insights into the Morphology Effect of Ceria on the Catalytic Performance of NiO–PdO/CeO2 Nanoparticles for Thermo-oxidation of n-C7 Asphaltenes under Isothermal Heating at Different Pressures. *Energy & Fuels* **2021**.
68. Mateus, L.; Moreno-Castilla, C.; López-Ramón, M. V.; Cortés, F. B.; Álvarez, M. Á.; Medina, O. E.; Franco, C. A.; Yebra-Rodríguez, Á., Physicochemical characteristics of calcined MnFe2O4 solid nanospheres and their catalytic activity to oxidize para-nitrophenol with peroxymonosulfate and n-C7 asphaltenes with air. *Journal of Environmental Management* **2021,** 281, 111871.
69. Medina, O. E.; Gallego, J.; Redondo, J. D.; Corteś, F. B.; Franco, C. A., Effect of pressure on the thermo-oxidative behavior of saturates, aromatics, and resins (S-Ar-R) mixtures. *Fuel* **2021**, 122787.
70. Medina, O. E.; Gallego, J.; Olmos, C. M.; Chen, X.; Cortés, F. B.; Franco, C. A., Effect of Multifunctional Nanocatalysts on n-C7 Asphaltene Adsorption and Subsequent Oxidation under High-Pressure Conditions. *Energy Fuels* **2020,** 34, (5), 6261.
71. Medina, O. E.; Gallego, J.; Nassar, N. N.; Acevedo, S. A.; Cortés, F. B.; Franco, C. A., Thermo-Oxidative Decomposition Behaviors of Different Sources of n-C7 Asphaltenes at High-Pressure Conditions. *Energy Fuels* **2020,** 34, (7), 8740.
72. Medina, O. E.; Gallego, J.; Cespedes, S.; Nassar, N. N.; Montoya, T.; Corteś, F. B.; Franco, C. A., Effect of pressure on thermo-oxidative reactions of saturates, aromatics, and resins (S-Ar-R) from extra-heavy crude oil. *Fuel* **2021**, 122596.
73. Rodriguez Acevedo, E.; Cortés, F. B.; Franco, C. A.; Carrasco-Marín, F.; Pérez-Cadenas, A. F.; Fierro, V.; Celzard, A.; Schaefer, S.; Cardona Molina, A., An enhanced carbon capture and storage Process (e-CCS) applied to shallow reservoirs using nanofluids based on nitrogen-rich carbon Nanospheres. *Materials* **2019,** 12, (13), 2088.
74. Hurtado, Y.; Franco, C. A.; Riazi, M.; Cortés, F. B., Improving the stability of nitrogen foams using silica nanoparticles coated with polyethylene glycol. *Journal of Molecular Liquids* **2020,** 300, 112256.
75. Hunger, B.; Heuchel, M.; Clark, L. A.; Snurr, R. Q., Characterization of acidic OH groups in zeolites of different types: An interpretation of NH3-TPD results in the light of confinement effects. *The Journal of Physical Chemistry B* **2002,** 106, (15), 3882-3889.
76. Martins, G.; Berlier, G.; Bisio, C.; Coluccia, S.; Pastore, H.; Marchese, L., Quantification of Brønsted acid sites in microporous catalysts by a combined FTIR and NH3-TPD study. *The Journal of Physical Chemistry C* **2008,** 112, (18), 7193-7200.
77. Márquez, S. B.; Cortés, F. B.; Marín, F. C., Desarrollo de Nanopartículas basadas en Sílice para la Inhibición de la Precipitación/Depositación de Asfaltenos. *Química y Petróleos; Universidad Nacional de Colombia: Medellín, Colombia* **2015**, 96.
78. Taborda, E. A.; Franco, C. A.; Lopera, S. H.; Castro, R. H.; Maya, G. A.; Idrobo, E. A.; Cortes, F. B. J. J. o. P. S.; Engineering, Effect of surface acidity of SiO2 nanoparticles on thermal stability of polymer solutions for application in EOR processes. **2021,** 196, 107802.
79. Hurtado, Y.; Beltran, C.; Zabala, R. D.; Lopera, S. H.; Franco, C. A.; Nassar, N. N.; Cortes, F. B. J. E.; fuels, Effects of surface acidity and polarity of SiO2 nanoparticles on the foam stabilization applied to natural gas flooding in tight gas-condensate reservoirs. **2018,** 32, (5), 5824-5833.
80. Plaza, M.; Pevida, C.; Arenillas, A.; Rubiera, F.; Pis, J., CO2 capture by adsorption with nitrogen enriched carbons. *Fuel* **2007,** 86, (14), 2204-2212.
81. Sharma, P.; Seong, J.-K.; Jung, Y.-H.; Choi, S.-H.; Park, S.-D.; Yoon, Y. I.; Baek, I.-H., Amine modified and pelletized mesoporous materials: Synthesis, textural–mechanical characterization and application in adsorptive separation of carbondioxide. *Powder technology* **2012,** 219, 86-98.
82. Wang, X.; Chen, L.; Guo, Q., Development of hybrid amine-functionalized MCM-41 sorbents for CO2 capture. *Chemical Engineering Journal* **2015,** 260, 573-581.
83. Monash, P.; Pugazhenthi, G., Investigation of equilibrium and kinetic parameters of methylene blue adsorption onto MCM-41. *Korean Journal of Chemical Engineering* **2010,** 27, (4), 1184-1191.
84. Du, Y.; Du, Z.; Zou, W.; Li, H.; Mi, J.; Zhang, C., Carbon dioxide adsorbent based on rich amines loaded nano-silica. *Journal of colloid and interface science* **2013,** 409, 123-128.
85. Wilfong, W. C.; Srikanth, C. S.; Chuang, S. S., In situ ATR and DRIFTS studies of the nature of adsorbed CO2 on tetraethylenepentamine films. *ACS applied materials & interfaces* **2014,** 6, (16), 13617-13626.
86. Mukherjee, S.; Samanta, A. N., Amine-impregnated MCM-41 in post-combustion CO2 capture: Synthesis, characterization, isotherm modelling. *Advanced Powder Technology* **2019,** 30, (12), 3231-3240.
87. Post, P.; Wurlitzer, L.; Maus-Friedrichs, W.; Weber, A. P., Characterization and applications of nanoparticles modified in-flight with silica or silica-organic coatings. *Nanomaterials* **2018,** 8, (7), 530.
88. Wong, H.; Iwai, H.; Kakushima, K.; Yang, B. L.; Chu, P., XPS study of the bonding properties of lanthanum oxide/silicon interface with a trace amount of nitrogen incorporation. *Journal of the Electrochemical Society* **2009,** 157, (2), G49.
89. Aranovich, G.; Donohue, M., Analysis of adsorption isotherms: Lattice theory predictions, classification of isotherms for gas–solid equilibria, and similarities in gas and liquid adsorption behavior. *Journal of colloid and interface science* **1998,** 200, (2), 273-290.
90. dos Santos, T. C.; Bourrelly, S.; Llewellyn, P. L.; Carneiro, J. W. d. M.; Ronconi, C. M., Adsorption of CO 2 on amine-functionalised MCM-41: experimental and theoretical studies. *Physical Chemistry Chemical Physics* **2015,** 17, (16), 11095-11102.

91. Serna-Guerrero, R.; Da'na, E.; Sayari, A., New insights into the interactions of CO2 with amine-functionalized silica. *Industrial & Engineering Chemistry Research* **2008,** 47, (23), 9406-9412.
92. Brunelli, N. A.; Didas, S. A.; Venkatasubbaiah, K.; Jones, C. W., Tuning cooperativity by controlling the linker length of silica-supported amines in catalysis and CO2 capture. *Journal of the American Chemical Society* **2012,** 134, (34), 13950-13953.
93. Loganathan, S.; Tikmani, M.; Mishra, A.; Ghoshal, A. K., Amine tethered pore-expanded MCM-41 for CO2 capture: Experimental, isotherm and kinetic modeling studies. *Chemical Engineering Journal* **2016,** 303, 89-99.
94. Aresta, M., *Carbon dioxide recovery and utilization*. Springer Science & Business Media: 2003.
95. Sim, K.; Lee, N.; Kim, J.; Cho, E.-B.; Gunathilake, C.; Jaroniec, M., CO2 adsorption on amine-functionalized periodic mesoporous benzenesilicas. *ACS applied materials & interfaces* **2015,** 7, (12), 6792-6802.
96. Caplow, M., Kinetics of carbamate formation and breakdown. *Journal of the American Chemical Society* **1968,** 90, (24), 6795-6803.
97. Ahmed, S.; Ramli, A.; Yusup, S., CO2 adsorption study on primary, secondary and tertiary amine functionalized Si-MCM-41. *International Journal of Greenhouse Gas Control* **2016,** 51, 230-238.
98. Chen, C.-H.; Shimon, D.; Lee, J. J.; Didas, S. A.; Mehta, A. K.; Sievers, C.; Jones, C. W.; Hayes, S. E., Spectroscopic characterization of adsorbed 13CO2 on 3-aminopropylsilyl-modified SBA15 mesoporous silica. *Environmental Science & Technology* **2017,** 51, (11), 6553-6559.
99. Gangarapu, S.; Marcelis, A. T.; Zuilhof, H., Carbamate stabilities of sterically hindered amines from quantum chemical methods: Relevance for CO2 capture. *ChemPhysChem* **2013,** 14, (17), 3936-3943.
100. Azmi, A.; Aziz, M., Mesoporous adsorbent for CO2 capture application under mild condition: a review. *Journal of Environmental Chemical Engineering* **2019,** 7, (2), 103022.
101. Ko, Y. G.; Shin, S. S.; Choi, U. S., Primary, secondary, and tertiary amines for CO2 capture: Designing for mesoporous CO2 adsorbents. *Journal of colloid and interface science* **2011,** 361, (2), 594-602.
102. Vaidya, P. D.; Kenig, E. Y., Acceleration of CO2 reaction with N, N-diethylethanolamine in aqueous solutions by piperazine. *Industrial & engineering chemistry research* **2008,** 47, (1), 34-38.
103. Donaldson, T. L.; Nguyen, Y. N., Carbon dioxide reaction kinetics and transport in aqueous amine membranes. *Industrial & Engineering Chemistry Fundamentals* **1980,** 19, (3), 260-266.
104. Hao, B. N.; Guo, Y. X.; Liu, Y. D.; Wang, L.-M.; Choi, H. J., Highly transparent electrorheological fluids of silica nanoparticles: the effect of urea modification. *Journal of Materials Chemistry C* **2016,** 4, (33), 7875-7882.
105. Karimi, S.; Mortazavi, Y.; Khodadadi, A. A.; Holmgren, A.; Korelskiy, D.; Hedlund, J., Functionalization of silica membranes for CO2 separation. *Separation and Purification Technology* **2020,** 235, 116207.
106. Nobarzad, M. J.; Tahmasebpoor, M.; Imani, M.; Pevida, C.; Heris, S. Z., Improved CO2 adsorption capacity and fluidization behavior of silica-coated amine-functionalized multi-walled carbon nanotubes. *Journal of Environmental Chemical Engineering* **2021,** 9, (4), 105786.
107. López, D.; Jaramillo, J. E.; Lucas, E. F.; Riazi, M.; Lopera, S. H.; Franco, C. A.; Cortés, F. B., Cardanol/SiO2 Nanocomposites for Inhibition of Formation Damage by Asphaltene Precipitation/Deposition in Light Crude Oil Reservoirs. Part II: Nanocomposite Evaluation and Coreflooding Test. *ACS omega* **2020,** 5, (43), 27800-27810.
108. Busch, A.; Gensterblum, Y., CBM and CO2-ECBM related sorption processes in coal: a review. *International Journal of Coal Geology* **2011,** 87, (2), 49-71.
109. Gabrielli, P.; Gazzani, M.; Mazzotti, M., The role of carbon capture and utilization, carbon capture and storage, and biomass to enable a net-zero-CO2 emissions chemical industry. *Industrial & Engineering Chemistry Research* **2020,** 59, (15), 7033-7045.
110. Gough, C.; Upham, P., Biomass energy with carbon capture and storage (BECCS): a review. *Tyndall Centre for Climate Change Research, Working Paper* **2010,** 147.
111. Ashley, M.; Magiera, C.; Ramidi, P.; Blackburn, G.; Scott, T. G.; Gupta, R.; Wilson, K.; Ghosh, A.; Biswas, A., Nanomaterials and processes for carbon capture and conversion into useful by-products for a sustainable energy future. *Greenhouse gases: science and technology* **2012,** 2, (6), 419-444.
112. Roy, K. S.; Naik, A. K., Recent Development of Novel Composite Materials for Carbon Capture: A Green Technology. *Green Innovation, Sustainable Development, and Circular Economy* **2020**, 3-16.